Hindawi
Advances in Materials Science and Engineering
Volume 2018, Article ID 4920718, 18 pages
https://doi.org/10.1155/2018/4920718

Review Article

A Review on Melt-Pool Characteristics in Laser Welding of Metals

Behzad Fotovvati, Steven F. Wayne, Gladius Lewis, and Ebrahim Asadi

Department of Mechanical Engineering, The University of Memphis, Memphis, TN 38152, USA

Correspondence should be addressed to Ebrahim Asadi; easadi8@yahoo.com

Received 14 November 2017; Revised 26 February 2018; Accepted 7 March 2018; Published 2 April 2018

Academic Editor: Paolo Ferro

Laser welding of metals involves with formation of a melt-pool and subsequent rapid solidification, resulting in alteration of properties and the microstructure of the welded metal. Understanding and predicting relationships between laser welding process parameters, such as laser speed and welding power, and melt-pool characteristics have been the subjects of many studies in literature because this knowledge is critical to controlling and improving laser welding. Recent advances in metal additive manufacturing processes have renewed interest in the melt-pool studies because in many of these processes, part fabrication involves small moving melt-pools. The present work is a critical review of the literature on experimental and modeling studies on laser welding, with the focus being on the influence of process parameters on geometry, thermodynamics, fluid dynamics, microstructure, and porosity characteristics of the melt-pool. These data may inform future experimental laser welding studies and may be used for verification and validation of results obtained in future melt-pool modeling studies.

1. Introduction

Laser is a coherent single-phase beam of lights from a single wavelength (monochromatic) with low beam divergence and high energy content, which creates heat when it strikes a metal surface. The advent of high-power (multi-kW) lasers in the 1970s [1] opened the door to many metal working applications, which, previously, had been done using conventional high-flux heat sources, such as reacting gas jets, electric discharges, and plasma arcs. One metal working application of lasers is laser welding, which requires power density $> 10^3\,\mathrm{kW{\cdot}cm^{-2}}$ [2]. In laser welding, two adjacent or stacked metal pieces are fused together by melting the parts at the weld line; usually, the process is conducted under an inert gas flow with or without addition of material to the weld line. The moving melted volume is called the melt-pool (Figure 1). The size of this pool, which is on the order of 1 mm, is influenced by many variables, such as the material, laser power, and welding speed.

The deep volume directly under the laser focus area is called the keyhole, within which the high energy of the laser creates heating rates $>10^9\,\mathrm{K{\cdot}s^{-1}}$ [3]. Thus, the material in the keyhole is rapidly melted and even boiled, thereby creating a metallic plasma around it. Boiling of the material maximizes the absorption of the laser energy by the material because it turns the keyhole to a black body [4]. The amount of absorbed energy in the material decreases exponentially through the thickness, as predicted by the Beer–Lambert law. A smaller portion of the absorbed energy is conducted away through reradiation and convection from the surface, while the rest is conducted into the substrate. An intense recoil pressure created by evaporation of the material in the keyhole generates a vapor jet and a fluid flow in the keyhole and the melt-pool (Figure 1) [5]. In addition, the surrounding area of the melt-pool that is still in the solid state will reach temperatures high enough to change the microstructure of the material or to cause solid-state phase transformation, depending on the material thermodynamics. This area is called the heat-affected zone (HAZ). Hereafter, we use the term "melt-pool" to refer to the combination of the keyhole, the molten-metal area (MMA), and the HAZ. Laser welding mechanisms can be divided into two categories based on the existence of the keyhole: keyhole mode and conduction mode. Keyhole-mode welding is more common because it produces narrow HAZs. However, keyhole oscillations and closures result in instabilities of the melt-pool, leading to creation of pores in the welded zones. On the other hand, there is more stability

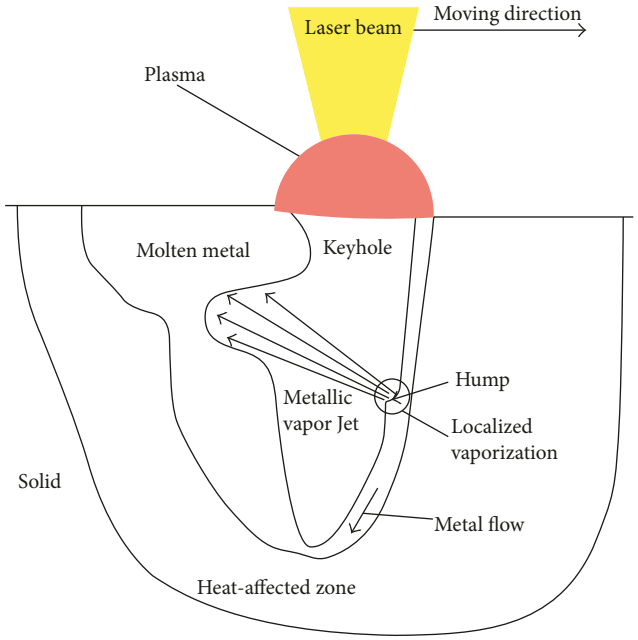

FIGURE 1: A cross-sectional schematic of a side view (the interface between two solids) of the melt-pool formed during a laser welding process.

in the conduction mode since vaporization is minimal. Conduction-mode welds are produced using low-power laser beams; as such, these welds are shallower than keyhole-mode welds [6]. The focus of this review is keyhole-mode laser welding.

Melt-pool characteristics directly control the quality of the weld, for example, porosity in the weld through keyhole thermodynamics and residual stresses through HAZ thermomechanics. As a result, one of the main goals of many research studies is to understand the relationships between weld quality and laser welding process parameters (such as laser type and laser power), substrate temperature, and melt-pool characteristics [7–12]. There are different types of lasers, three widely used ones being neodymium-doped yttrium aluminum garnet (Nd:YAG), CO_2, and argon lasers. Lasers differ in characteristics, such as maximum output power and pulse repetition rate that they can provide, and, as such, the choice of the laser should be based on the application being considered. For instance, Morgan et al. [13] conducted density analysis experiments on 316L stainless steel and chose Nd-YAG laser over CO_2 laser due to increased absorption of a 1.064 μm wavelength by metallic powder compared to a longer wavelength (10.64 μm) [14].

Locke et al. [15] carried out one of the early experiments on laser welding of metals. They used laser power levels of 8 kW and 20 kW, leading to penetration depth and speed that had not been possible previously. The penetration depth achieved was 12.7 mm at a ratio of 2.54 m·min^{-1} in a 5-to-1 depth-to-average-width fusion zone in 304 stainless steel at a 20 kW laser power level. The state of the art of laser welding of metals and associated melt-pool characteristics in those early days of research was reviewed by Mazumder in 1982 [2] and in 1987 [16]. Since then, laser welding of metals has advanced significantly in many aspects, such as welding materials, process monitoring, computational modeling, and quality. There are a few review papers in the literature that deal with recent advancements in laser welding of metals. In 1989, David and Vitek [17] focused on the solidification behavior of the melt-pool and investigated the correlation between the weld metal microstructure and solidification parameters such as crystal growth rates and the consequent interface cooling rates. They presented a diagram showing the variation of weld microstructure as a function of cooling rate, growth rate, and combination(s) of these variables. In 2003, Cao et al. [18, 19] reviewed research and progress in laser welding of wrought Al alloys. They reviewed findings regarding the influence of an assortment of parameters, which they divided into three categories (laser-, process-, and material-related parameters), on weld quality. They quantified the weld quality by metallurgical microstructures and defects, such as porosity, cracking, oxide inclusions, and loss of alloying elements, as well as mechanical properties of the weld, such as hardness, tensile strength, fatigue strength, and formability. In 2005, Shao and Yan [20] reviewed on-the-fly monitoring techniques for inspecting the laser welding process, highlighting the advantages and limitations of acoustic, optical, visual, thermal, and ultrasonic techniques. In 2006, Cao et al. [21] conducted a similar review but focused on Mg alloys. In 2014, Liu et al. [22] reviewed laser welding studies of dissimilar Mg and Al alloys. Their review also included discussion of progress on research on other welding techniques applied to these alloys, including solid-state processes and fusion welding. The authors stated that a challenge in welding dissimilar Mg and Al alloys is the formation of brittle intermetallic compounds, which can be addressed by eliminating or reducing the Mg-Al intermetallic reaction layer through careful selection of process parameters.

Modeling the laser welding process has been another major research focus. This is challenging due to the multiphysics nature of the problem (Figure 1); that is, it involves laser-material interaction, fluid flow, large temperature variation, plasma formation, vapor-liquid-solid coexistence, and possible solid-state phase transformation [4, 23–25]. As analytical solution of the laser welding process is not possible (except in the case of a simplified physics and geometry model), numerical/computational approaches have been taken. In 2005, Mackwood and Crafer [26] reviewed the literature on thermal modeling up to 2002. They divided the work conducted into categories based on the welding method, such as arc, resistance, and friction, as well as welding processes, such as alloying, cladding, and surface hardening. The review covered basic analytical solutions, such as a moving/fixed-point heat source combined with a line source of heat, along with numerical solutions, including standard heat transfer solutions, welding dissimilar metals, multipass welding, melt-pool models, and keyhole models. Also, in 2005, Yaghi and Becker [27] reviewed thermal and mechanical welding simulations in which finite element analysis (FEA) was used. The simulations included heat flow processes and solid-state phase transformations occurring in the welding process. They discussed several

relevant modeling considerations (such as parametric studies of residual stresses), influence of material properties on residual stresses, and combination of welding simulation with other heat transfer engineering processes. In 2012, He [28] updated the review of FEA studies on laser welding, with special attention to the simulation of defect formation. He discussed numerical problems in FEA of laser welding, including materials modeling, meshing procedure, and failure criteria. He concluded that establishing an accurate and reliable finite element model of laser welding is very difficult because the process is a complex phenomenon that comprises many interrelated mechanisms and metallurgical processes. In 2015, Svenungsson et al. [29] conducted a review of modeling investigations of the keyhole and categorized these models based on the considerations and assumptions used in constructing the models.

Most reviews on laser welding are limited to either a specific material or method of study, namely, experimental, on-the-fly monitoring, or computational. In other words, there is no review on the state of the art on the properties of the melt-pool and their relationship to the welding process parameters and weld quality. In the present review, we focus on these aspects. Thus, the present review focuses on the following melt-pool characteristics: (1) geometrical features, such as the penetration depth, width, HAZ geometry, keyhole geometry, and MMA geometry; (2) thermodynamic characteristics, such as laser energy absorption, surface temperature, cooling rates, and temperature map in the melt-pool; (3) fluid dynamic characteristics, such as fluid flow in the melt-pool and vaporization in the keyhole; (4) resulting microstructures; and (5) porosity characteristics, including factors that influence porosity formation and methods to avoid it. Due to the multiphysics and integrated nature of the melt-pool, in some literature reports, there may be some overlap coverage of the abovementioned aspects. In each section of the present review, we critically discuss the state of the art in determination of the considered melt-pool characteristic, its variation with process parameters, and its influence on commonly used weld quality quantifiers, such as the microstructure and mechanical properties. In the final section, we summarize the key points made and identify some gaps in the reviewed models of laser welding of metals that hinder full characterization of the process.

2. Melt-Pool Geometry

The magnitude and distribution of cooling rates, temperature, and the maximum thickness that can be achieved by a single welding pass are determined by the melt-pool geometry [7]. Additionally, the microstructure of the fusion zone is also influenced by the melt-pool geometry. There are several studies on the influence of laser power and welding speed on melt-pool geometrical features (Table 1). A summary of optimum laser welding process parameters, for a selection of metals and alloy materials, is given in Table 2. Summaries of studies on the influence of laser welding process variables on melt-pool and keyhole features are presented in Appendix.

Table 1: Influence of two laser welding parameters on various melt-pool geometry parameters.

Geometry parameter	Process parameter	
	Laser power	Welding speed
Melt-pool depth	$+^{a}$	$-^{b}$
Melt-pool width	$+^{c}$	$-^{d}$
Melt-pool depth/width ratio	NS	$+^{e}$
Melt-pool length	$+^{f}$	$-^{g}$
Keyhole radius	$+^{g}$	$-^{g}$
Cooling rate	$-^{h}$	$+^{i}$
Melt-pool surface area	$+^{j}$	$-^{k}$
Vaporization rate	$+^{l}$	NS

$^{+}$Direct relationship; $^{-}$inverse relationship; NS: not stated in the report; [a][11, 30–37]; [b][11, 31, 33, 38–41]; [c][11, 33–37, 42–44]; [d][11, 12, 31, 33, 38, 41, 42, 45]; [e][30]; [f][32, 42]; [g][42, 45]; [h][7, 8]; [i][8]; [j][43, 46]; [k][38, 41, 47]; [l][44, 46].

In laser welding applications, the maximum achievable welding speed is limited by the maximum available laser power. For economic reasons, it is desirable to apply the highest possible speed during laser welding, while a full penetration is achieved at the same time. A feedback controller, in which an optical sensor measures the intensity of the melt-pool radiation and exports it to a feedback control system, has been described by Postma et al. [48]. They also proposed a dynamic model, which describes the sensor and laser source dynamics, using system identification techniques. This model, which uses laser power as the input and the modeled sensor signal as the output, is capable of maintaining full penetration in the presence of artificial power variations and speed changes. This procedure optimizes the welding speed without risking lack of penetration.

Surface structure and hardness of the substrate after laser-related processes are also affected by process parameters. Ashby and Easterling [52] conducted experiments and combined the equations of heat flow and kinetics to evaluate the near-surface structure and hardness after laser treatment. Using a Gaussian heat source for their model, they presented diagrams, which show the structure and the hardness of the surface, as a function of process parameters. Using these diagrams, the maximum achievable surface hardness without surface melting that results from using an optimum combination of process parameters is identified.

In the process of deep penetration welding, a high energy density is transferred to the workpiece through the keyhole; therefore, the flows of metal vapor inside the keyhole and the molten material around it play an important role in the welding process, and the shape of the keyhole would highly affect the weld quality. One approach that is employed to evaluate the shape of the keyhole in this process is to estimate its cross-sectional area in each depth. The model presented by Dowden et al. [53] utilized this approach. They assigned a single temperature to vapor materials. Therefore, by obtaining the temperature distribution in each depth, a border between the vapored materials and the materials that are not vapored could be distinguished as the keyhole. The keyhole shape that they obtained was one that has a circular cross section with a curved axis. Steen et al. [54]

Table 2: Optimum laser welding parameters for a selection of metals and alloys.

Metal/alloy	Parameter			
	Laser power (kW)	Welding speed ($m \cdot min^{-1}$)	Focal position (relative to the surface) (mm)	Shielding gas
Mg alloy, WE43 [11]	2	2	0 or −1	Helium
Mg alloy, AZ91 [11]	2	3	0	Helium
Several Mg alloys [49]	1.5[a] 2–2.5[b]	2.5–3[a] 1-2[b]	−2	Helium
Ti-6Al-4V alloy [50]	NS	0.8	NS	Helium
Stainless steel 304L [30]	4	3	0.2	Helium
Stainless steel 347 [30]	5	2	0.4	Helium
Stainless steel 304 [33]	1.25	0.75	NS	NS
Galvanized steel [34]	1.3	1	NS	Argon
Inconel 625 [39]	1.5	2	NS	NS
Zn and Sn [51]	1.6	1.5	5	NS
Stainless steel 440 and 416 [35]	Any combination of parameters that produces energy density in the range of 20.8 to 27.7 $J \cdot mm^{-2}$			

NS: not stated in the report; [a]for thinner plates (2.5 mm and 3.0 mm); [b]for thicker plates (5.0 mm and 8.0 mm).

employed another approach to estimate the keyhole shape by the combination of a point heat source and a line heat source. They found a simple analytical form for the temperature distribution, and possible weld profiles were found numerically with specific choices for the strengths of the line and point sources and specific locations for the point source. Comparison of the obtained profiles with the actual measured profile led to the profile that gave the best fit, leading to magnitudes of the line and point sources and the point source location.

Beck et al. [55] used the equations of continuity, motion, and energy to obtain the velocity and temperature fields and, hence, the keyhole shape and the maximum velocity of the melt flow at the sides of the keyhole. Kaplan [56] employed another technique to obtain the keyhole shape. He used the energy balance point-by-point through the substrate thickness to find the position of each point of the keyhole profile. This work showed that most of the laser beam heat was absorbed at the front wall of the keyhole rather than at the rear wall. Lampa et al. [57] simplified Kaplan's model and used it for calculating the penetration depth, by applying a correction factor for the material conductivity at the top of the melt-pool. The correction factor was calculated as 2.5, which makes the material more conductive.

Amara and Bendib [58] solved the Navier–Stokes equations for an incompressible fluid flow concentrated on the vapor pressure in the keyhole and confirmed that the vapor pressure works against forces, such as surface tension, that tend to close the keyhole opening. They used the ray-tracing code, which allows calculation of the energy deposited on the keyhole wall after each reflection of the laser beam. However, Fabbro et al. [59] showed that due to the high absorptivity of the front keyhole surface (60% to 80%), only one reflection of the laser beam is necessary for the modeling. Tenner et al. [60] used another method to estimate the keyhole shape, that is, by relating it to the plasma plume. Through experiments, they showed that the keyhole dynamic behavior is well correlated with the plume when a threshold laser power is reached, with this power being ~80% of the power required for full penetration (in this case, 2.5 kW). They concluded that, at low laser powers, the stability of the keyhole is determined by the evaporation process in the keyhole. Fabbro [61] defined some regimes in laser welding and investigated the keyhole shape, particularly, the keyhole front wall tilting, in the different regimes. They observed that, at low welding speeds, the keyhole is more unstable, and the intensity, which is absorbed by the keyhole front wall, depends on the welding speed, not the intensity itself. Postacioglu et al. [62] estimated the shape of the surface of the weld as elevated or depressed. Kar and Mazumder [63] used mass conservation, momentum, and energy equations along with the heat transfer in the solid and vapor phases of the materials to predict the shape of the melt-pool by calculating the surface velocity and temperature distribution. They observed that the axial velocity at the beginning of the laser melting process is negligible, compared to velocities in other directions; however, after keyhole development, the dominant velocity is in the axial direction. They asserted that the moving speed of the solid-liquid interface is much higher than that of the liquid-vapor interface; in other words, the melt-pool depth increases more rapidly than does the keyhole depth.

3. Melt-Pool Thermodynamics

Heat transfer in the melt-pool during laser welding significantly affects the melt-pool shape, melt flow inside the melt-pool, and cooling rates of the melt-pool and, thus, the quality and microstructure of the weld [64]. Since, in laser welding, dimensions of the melt-pool are on the order of mm and timescales are on the order of fractions of a second, measuring the temperature profiles and cooling rates of each point is costly and time-consuming. Thus, many of the studies reported on the thermodynamic characteristics of the melt-pool during laser welding are modeling works.

Mazumder and Steen [4] developed a three-dimensional quasi-steady heat transfer model of laser melting and compared their results using this model to those obtained from experiments. For simplicity, they assumed that there is no reflectivity at the material surface, where the temperature

exceeds the boiling temperature of the material and the thermal properties of the material are constant and independent of temperature changes. Using this model, some process parameters were predicted, including the temperature profile, maximum welding speed, HAZ width, thermal cycle at any location or speed, and the effect of supplementary heating or cooling, thickness, reflectivity, and thermal conductivity on the melt-pool shape.

Goldak et al. [65] presented a more sophisticated model of weld heat sources that consisted of two combined ellipsoid shapes and is flexible enough to change the size and the shape of the heat source so that it could be used for shallow or deep penetration welding with various types of heat sources, such as arc, laser, and electron beam. They observed some differences between FEA and experimental results and suggested the reason to be due to neglecting the heat flow in the longitudinal direction. They found that the energy losses due to radiation and convection near the heat source are negligible.

Wang et al. [66] considered continuity, energy, and momentum equations and employed the volume of fluid method [67], which can be used to calculate the free surface shape of the keyhole, to solve a three-dimensional model of the temperature distribution. Using assumptions that the material properties are constant and the fluid flow is laminar and incompressible during the process, they found large temperature gradients in the front region of the keyhole. They claimed that the recoil pressure is the main driving force for the keyhole formation. Akbari et al. [68] used the same sets of equations and assumed the melt-pool surface to be flat and the fluid flow to be transient, laminar, and incompressible. They found that regardless of the welding speed, the temperature distribution decreased sharply at the laser beam center and then decreased slightly far away from the center of the laser beam. Frewin and Scott [69] considered temperature dependence of material properties and stated that the temperature profile is a function of absorptivity and laser beam energy distribution. De et al. [70] assumed a double-ellipsoidal model for the heat source to present a two-dimensional conduction heat transfer model. They investigated the effect of varying the penetration depth and absorptivity on the exactness of the model results.

Vaporization is important in laser welding of alloys that contain one or more volatile constituents because vaporization determines the thermodynamic characteristics of the melt-pool. Khan and Debroy [44] concluded that the relative rate of vaporization of any two elements from the melt-pool was an indicator of melt-pool temperature, irrespective of the element pair selected. Increasing the laser power will increase the vaporization rate by increasing the temperature and the surface area of the melt-pool. Collur et al. [71] conducted several experiments to examine the role of gas-phase mass transfer in the vaporization of alloying elements and modeled the role of plasma in the vaporization of alloying elements. The melt-pool is surrounded by a plasma during laser welding, allowing molten metal drops to vaporize, both in the presence and absence of plasma, isothermally. They found that, under various shielding gas environments, the rate of vaporization of alloying elements is independent of the flow rate and also of the nature of the shielding gas but is controlled by plasma-influenced intrinsic vaporization at the melt-pool surface.

To simplify modeling convection in the melt-pool, many researchers assumed that the thermal conductivity of the material is isotropic in that region [24, 72, 73]. In contrast, Safdar et al. [74] took into account the anisotropic thermal conductivity and stated that the anisotropy-enhanced thermal conductivity approach leads to a more accurate result in the prediction of melt-pool temperature distribution.

There are many parameters that affect the shape of the melt-pool. One of them is the Marangoni convection, also called surface tension-driven convection, which is convection along an interface between two fluids due to a surface tension gradient [75]. Tsotridis et al. [76] presented a simplified model of the melt-pool considering the Marangoni convection. For simplicity, they assumed that all the physical properties of the solid and the liquid are the same, and they claimed that the Marangoni flow dominated over the buoyancy flow. Tsai and Kou [73] presented a two-dimensional heat transfer fluid flow model to describe the Marangoni convection in the melt-pool that is dependent on the surface tension temperature coefficient. They asserted that when this parameter has a negative value, the Marangoni convection direction is radially outward, and the pool center is depressed but the outer part is elevated. However, a positive coefficient results in a convex melt-pool.

Limmaneevichitr and Kou [43] conducted experiments to investigate the effect of the Marangoni convection on the melt-pool shape. In this work, they used $NaNO_3$ and Ga for welding as these two materials have extremely high and low Prandtl number (Pr), respectively; $\mathrm{Pr} = C_p\mu/k$, where C_p is the specific heat, μ is the dynamic viscosity, and k is the thermal conductivity. The Peclet number (Pe) is also important in determining the effect of the Marangoni convection. Pe expresses the ratio of heat transport by convection to heat transport by conduction; that is, $\mathrm{Pe} = LV/\alpha$, where L is the pool surface radius, V is the maximum outward surface velocity, and α is the thermal diffusivity. For the melt-pools of $NaNO_3$, a material with a high Pr, α is very low and V is high (strong Marangoni convection). Therefore, Pe is very high, and heat transport in the melt-pool is dominated by the Marangoni convection. Increasing the beam power increases the Marangoni convection, the melt-pool size, V, L, and, hence, Pe. Experimental results showed that if a strong outward surface flow carries the heat outward to the melt-pool edge, it makes a concave pool bottom wide and flat. Reducing the beam diameter also increases the Marangoni convection and Pe. The return flow penetrates the pool bottom close to the pool edge and turns the flat pool bottom to a convex one. Both the convex and flat pool bottoms indicate that the Marangoni convection dominates over buoyancy convection, which is induced by gravity in the pools. On the other hand, for melt-pools of Ga, Pe is very low, and conduction dominates heat transport in the melt-pool. Heat is conducted downward and outward and, thus, makes the pool bottom concave. Reducing the beam diameter makes the melt-pool more hemispherical, which confirms the domination of conduction over heat transport in the pool.

Yang et al. [9] presented a model by combining continuity, momentum, and energy equations for liquid and solid phases and reported that the thermal properties of the material and the Marangoni flow in the melt-pool could significantly influence the melt-pool shape such that more Marangoni flow results in a wider and shallower melt-pool. Abderrazak et al. [10] utilized their experimental and finite volume simulation results obtained from Mg alloy specimens to assert that a negative Marangoni effect, due to the absence of the surface active agent in the alloy composition, makes the melt-pool wider and shallower.

The physical origin of the enhanced energy transfer from a laser to a material may be explained on the basis of two alternative mechanisms, namely, Fresnel absorption and inverse bremsstrahlung (IB) absorption [77]. The Fresnel equation describes the behavior of light when moving between media of differing refractive indices. The absorption of light that the equations predict is known as Fresnel absorption. IB absorption is one of the important mechanisms for transferring energy from laser light to matter. In the very intense field used in a laser fusion program, processes involving multiphoton absorption and emission are very important [78]. There have been a number of different formalisms suggested for treating IB in intense fields [79] together with a few numerical calculations [79]. For example, Zhang et al. [80] presented a sandwich model to observe the keyhole in deep penetration laser welding, thus providing an effective way to analyze both Fresnel and IB absorptions. By increasing the thickness of Al films between two glass pieces, higher densities of the keyhole plasma are achieved, leading to deep keyholes. By continuing to thicken the Al films, the aperture of the keyhole continues to widen. However, above a critical thickness, the depth of the keyhole reduces (in Al films, this critical thickness is 0.3 mm). This is due to the excess density of the keyhole plasma, which prevents the transmission of the laser beam to the keyhole. The density of the keyhole plasma creates similar effects on changes in welding depth compared to keyhole depth. Cheng et al. [77] computed the laser intensity absorbed on the keyhole wall using Fresnel and IB absorptions of the keyhole plasma. They concluded that IB absorption of the keyhole plasma plays a more important role than does Fresnel absorption. They asserted that the temperature of the keyhole plasma decreases from the top to the bottom of the keyhole and decreases from the center to the edge of the keyhole. Tan et al. [81] found that almost invariably, the maximum temperature in the keyhole wall is located at the bottom of the keyhole.

4. Melt-Pool Fluid Dynamics

In order to obtain a high-quality laser-welded metal product, it is necessary to prevent defects before they occur. When a metal is in the liquid state, the probability of collapsing of the melt-pool or its partial penetration is high. Therefore, the dynamics of the melt-pool and the fluid flow patterns are important.

Zacharia et al. [82] proposed that surface active elements may alter the flow field in the melt-pool and, hence, affect weld penetration. They showed that a combination of the concentration of the surface active elements and the temperature distribution has an important role in determining weld penetration. It was also shown that the melt-pool flow can be simulated more realistically considering not only the coefficient of surface tension as a function of temperature but also the concentration of the surface active elements. In laser welding (unlike gas tungsten arc welding [83, 84]), the latter factor makes the temperature coefficient of surface tension largely negative, causing the flow to be radially outward at the melt-pool surface. This flow transfers the heat out from the center of the melt-pool and makes the pool shallow.

Semak et al. [85] investigated the dynamics of the melt-pool by conducting experiments using three different types of pulses: a single 20 or 30 ms pulse, continuous wave pulse, and repetitive 20 ms pulses. They observed that the vaporization pressure exceeds surface tension and hydraulic pressure in the melt-pool, creating a high-velocity melt flow and, thus, a melt crown around the keyhole at the melt-pool edge. Also, significant variations in the shape of the keyhole opening were observed, which were attributed to the instability of the vapor pressure. Semak et al. [86] presented a model to simulate the fluid flow in the melt-pool during pulsed laser welding. In a later contribution, they modified their simulation to include the effect of surface tension [87]. They asserted that the effect of this force could be an ejection or a retention, depending on the distribution of the beam intensity.

Cho et al. [88] simulated the fluid flow in the melt-pool during the transition from conduction laser spot welding to keyhole laser spot welding and showed an upward and downward oscillation in the fluid flow in the center of the melt-pool in the direction of normal to the surface. They attributed this oscillation to interaction of competing pressures, including recoil pressure and surface tension pressure. Using a sandwich model, Zhang et al. [89] observed the dynamics of the keyhole and showed that the hydrodynamics at the keyhole wall have a dominant effect on defects in the weld. Geiger et al. [90] used continuity, heat conduction, and the Navier–Stokes equations to show how pores form at high welding speeds (such as $12\,\mathrm{m{\cdot}min^{-1}}$). A higher welding speed results in a higher pressure at the keyhole front and, thus, higher velocities of melt flow around the keyhole, which lead to a depression outside the keyhole. A combination of this phenomenon with the surface tension leads to formation of pores.

The coupling between the melt-pool and the keyhole is complicated. It has been shown that the sideways liquid displacement around the front keyhole wall is the main process for generating high velocities of the fluid that enters the melt-pool [25, 91]. Basu and DebRoy [92] found a threshold for the melt-pool surface temperature above which the vaporization-induced recoil pressure overcomes the surface tension pressure, causing an outward flow to the sides [93]. The recoil pressure is one of the three main mechanisms responsible for expelling melt from the keyhole. The other two, which are particularly important at higher melt surface temperatures, are melt evaporation and the

shielding gas interaction with molten metal. The melt flow generated by the recoil pressure has a direction in which the recoil pressure gradient is the highest. Therefore, in laser welding, the melt flow is ejected by the recoil pressure to the sides of the melt-pool [25]. Fabbro et al. [40] discussed the effects of the interaction between the vapor, which is generated by the ablation process occurring on the front keyhole wall, and the surrounding melt-pool. They showed that an efficient control of the dynamics of the melt-pool can be achieved using a side gas jet, which can be localized in the front or the rear position. This gas jet decouples the interaction zone inside the keyhole and the melt-pool. Therefore, the melt-pool flow can be well stabilized, resulting in a high-quality weld and improved penetration at low welding speeds. Amara and Fabbro [94] modeled the fluid flow in the melt-pool, considering the interaction between the vapor and the liquid and between the liquid and the air. Fabbro et al. [95] showed that the escaping vapor, which is generated in the keyhole, creates friction forces, which, in turn, play an important role in fluid flow in the melt-pool. Experiments [96] showed that these forces generate humping instabilities on the melt-pool above a critical welding speed. Amara et al. [97] considered the friction effects of the vapor flow with the liquid walls as an important factor to numerically solve the hydrodynamic equations, obtaining the shear stress distribution on the keyhole walls. Further investigations [98] lead to three-dimensional calculations of the molten metal flow velocity induced by the friction phenomenon and the thickness of the boundary layer. The friction force, which is induced on the melt-pool wall, results in a drag force expelling the flow towards the surface. The other main driving forces for the molten material in the melt-pool result from surface tension, recoil pressure, and buoyancy forces [5, 85, 94]. By solving a combination of the Navier–Stokes, energy conservation, and ideal gas equations, using the finite volume method, it was confirmed that using a gas jet during deep penetration laser welding results in better weld joints because the melt flow in the melt-pool is enhanced.

Insufficient metal flow in the melt-pool may be due to excessive welding speed or incorrect laser power, which leads to hump formation, a phenomenon that produces variation in weld penetration [99]. Once the hump starts to be solidified, further melt flows upwards and resolidifies, causing the hump to grow [100]. The travel angle between the laser beam and the welding direction has been found to affect the onset of humping. Forehand welding has been shown to suppress hump formation to higher welding speeds [101, 102]. Gratzke et al. [103] defined a critical ratio of the width to the length of the melt-pool, which determined the likelihood of hump formation, such that maximizing this ratio during welding decreases the possibility of hump formation. Another way of reducing humping defects in laser welding is by using a tandem dual beam [104]. When the beams are far apart, the second beam suppresses the humps formed by the first one, and when the beams are close, the following beam stabilizes the keyhole, thereby preventing hump formation after the leading beam. According to Beck et al. [55], any reduction in flow velocities in the rearward direction avoids hump formation. Kern et al. [105] used this concept in their experiments of CO_2 laser welding of steel by applying a magnetic field transverse to the welding direction, thus altering the melt flow profile within the melt-pool and suppressing hump formation. Matsunawa and Semak [106] simulated the keyhole during high-speed laser welding and found that hump formation frequency was increased with increasing welding speed. However, Kawahito et al. [107] defined a process window of welding speed and laser beam diameter, in which humping occurred over a particular range of laser power densities. In a later work [108], these authors found hump formation to be caused by several dynamic and static factors, including flow velocity, surface tension, solidification, and melt volume. They asserted that hump formation could be avoided in fully penetrated welds by decreasing melt volume so that the formation of the convex surface at the rear end of the melt-pool was suppressed. According to the model of Matsunawa and Semak [106], when the component of the keyhole velocity that is parallel to the surface was higher than the beam translation speed, the instability of the keyhole resulted in hump formation on the weld surface. A hump may also form on the keyhole wall surface when the upper part of the keyhole wall moves away from the laser beam axis and the lower part continues to move towards the axis. Ilar et al. [109] introduced root humping, which was different from top surface humping, being formed due to a gravity effect. Root humping was initiated by the increase in the amount of the material flowing in the melt-pool that originated from the bottom of the melt-pool. Amara and Fabbro [110] presented a 3D model based on the numerical resolution of the fluid flow and the heat transfer equations showing hump formation at high welding speeds in deep penetration laser welding. Pang et al. [111] found significant differences between melt-pool dynamics of an unstable keyhole and a stable one and that, by controlling the welding speed and surface tension, they could prevent the formation of humps on the keyhole wall, thus reducing keyhole instability. They stated that, under certain low-heat input welding conditions, collapse of the keyhole wall could be avoided.

Ki et al. [45, 112] presented a three-dimensional laser keyhole welding model and used the Navier–Stokes and energy equations to simulate the movements of the liquid-vapor interface and the solid-liquid interface as well as the heat transfer. In addition, they simulated the transition from conduction-mode welding to keyhole-mode welding. For the sake of simplicity, they extrapolated material properties at high temperatures from values obtained at lower temperatures. They did not take plasma into account, assumed the gas was incompressible, and neglected recondensation of the vapor after interacting with the hole surface. They confirmed that one of the main differences between the two types of laser welding (keyhole mode and conduction mode) is the recoil pressure, which is generated by evaporation during the laser keyhole welding. There is a fluctuation in the amount of laser energy absorbed in the keyhole, which, in turn, leads to fluctuation of the shape of the keyhole, and this fluctuation affects the recoil pressure and the flow field in the melt-pool. Their model also allows prediction of the

microstructure and property evolution in laser-welded joints. Chakraborty and Chakraborty [72] developed a three-dimensional model of laser welding using conservation of mass, momentum, and energy equations to evaluate the influence of turbulence in the melt-pool on the process parameters and found that the velocity and temperature gradients are smaller in the turbulent melt-pool, a finding that agrees with the experimental results.

5. Weld Microstructure

A high cooling rate typically is experienced by the melt-pool immediately after laser welding. Solidification takes place usually in a few tens of milliseconds, and metastable microstructures are produced that influence the final mechanical properties of the weld. Therefore, microstructure characterization is vital in the determination of weld quality [113, 114]. Solidification of molten weld metal depends on the kinetics of the liquid-solid interface. Kou [115] described this by using values of the thermal gradient (G) (usually, they are in the range of 100–1000 $K{\cdot}m^{-1}$) and the travel speed of the liquid-solid interface (R) (usually, they are in the range of 10–103 $m{\cdot}s^{-1}$). Kou identified four possible modes of solidification: (1) planar (high G and low R), (2) cellular, (3) columnar dendritic, and (4) equiaxed dendritic (low G and high R) (Figure 2). The ratio of G to R determines the mode of solidification. Kou showed that the product of G and R indicated the cooling rate, so these two parameters determined the fineness of the solidified microstructure (Figure 2). Kou also noted that solidification of the melt-pool could take place in one of two ways, namely, (a) epitaxial and (b) nonepitaxial, depending on the composition of the weld metal.

The microstructure of rapidly solidified laser-molten Al-4.5 wt.% Cu alloyed surfaces was studied, and melted regions were found to resolidify epitaxially onto unmolten crystalline substrates [116]. Solidification proceeded as follows: a plane front mode, then cellular, and, finally, continuing in a columnar competitive manner. The major impact of the rapid solidification was a refinement of the surface microstructure. Kou [115] found that melt convection was not sufficiently vigorous to produce a homogeneous melt. Evidence of epitaxial resolidification was also found in a nickel-based superalloy (Udimet 700) when laser melted [117]. This face-centered cubic (fcc) material showed a strong preference for dendritic growth along (100) directions. The consequence of the rapid cooling rate was evident by fine dendritic regrowth, with a spacing of ~2.5 mm. The dendrites grew nearly parallel to the local direction of maximum heat flow [117].

Many researchers have investigated the microstructures of welds in laser welding of stainless steels and other ferrous alloys. Zambon and Bonollo [118] characterized the microstructure of weld beads and the HAZ of austenite and duplex stainless steels. They stated that high cooling rates might result in formation of nonequilibrium microstructures, which contain larger amounts of δ-ferrite in duplex steels than predicted both by the Fe-Ni-Cr pseudobinary phase diagram and by the Schaeffler diagram.

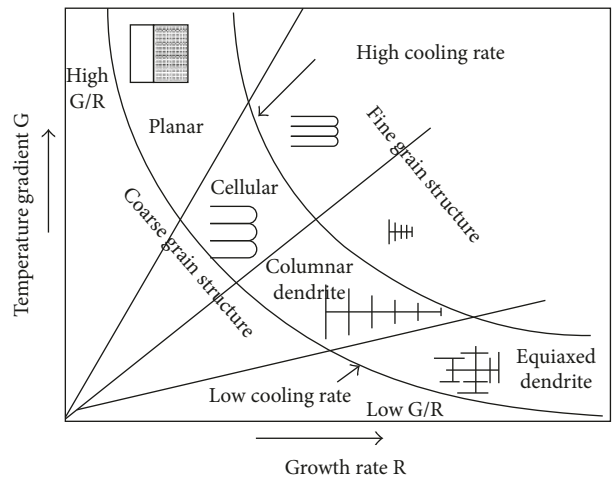

Figure 2: Influence of temperature gradient (G) and growth rate (R) on the mode of solidification and grain structure [115].

They concluded that nonequilibrium microstructures decreased the corrosion resistance of the welded joints. The rate at which a ferrous metal/alloy weldment cools significantly influences the ferrite morphology and distribution [119]. Zacharia et al. [8] presented a model to obtain the complex temperature distribution and the cooling rates and showed that, in pulsed laser welding, at low speeds, the weld metal remains molten, even during the time when the laser beam is not being applied. They confirmed that the microstructure is dependent on the cooling rates and ranged from duplex austenite + ferrite to fully austenitic or fully ferritic. These authors conducted another study in two parts (analytical and experimental) [82, 120] and by employing the equations of momentum, energy, and mass continuity concluded that the dominant force for the fluid flow is the surface tension gradient. They found the cooling rates at the solidification temperature to be the highest at the edge of the melt-pool rather than at the bottom or the top center of it. In another study by Zacharia et al. [82], their observed microstructural evaluation of laser-welded 304 stainless steel fusion zones revealed a fine dispersion of chromium oxide inclusions and a continuous oxide layer. The observed microstructures were sensitive to the cooling rates, with the decrease in the cooling rate resulting in a coarser solidification substructure with a widely spaced ferrite network. The rapid solidification of the laser beam-welded metal resulted in a fully austenitic microstructure with a fine solidification substructure. Lippold [121] determined the susceptibility of weld solidification cracking in austenitic stainless steels during pulsed laser welding. The author found that a shift in weld solidification behavior occurred under rapid solidification conditions. Solidification as primary austenite was found to be the most detrimental, and cracking depended mainly on composition, whereas pulsed laser welding process parameters had only a small influence. A solidification model was discussed that related the transition in primary solidification from ferrite to austenite to dendrite tip undercooling at high solidification growth rates.

Lippold [121] also found out that the available predictive microstructure diagrams and solidification models (the Suutala weldability diagram [122] and the Welding Research Council constitution diagram [123]) are not accurate under rapid solidification conditions, which happens during pulsed laser welding of stainless steels. Therefore, regarding rapid solidification, they proposed a predictive diagram for weld solidification cracking susceptibility, a solidification model relating the transition in primary solidification from ferrite to austenite to dendrite tip undercooling, and a microstructural map for austenitic stainless steel welds. Brooks et al. [124] studied high-energy stainless steel welds and concluded that minimal solid-state diffusion occurs during the solidification and cooling of primary austenite solidified welds, whereas structures which solidify as ferrite may become almost completely homogenized as a result of diffusion. A nearly segregation-free, single-phase austenite structure, which appears to be unique to the rapid solidification velocities and cooling rates of high-energy welds, was also observed. They suggested that this structure was a product of a marked phase transformation in which ferrite was transformed to austenite.

Recently, marked transformations were identified in the selective electron beam melting of Ti-6Al-4V. Thus, Lu et al. [125] concluded that the β (body-centered cubic (bcc)) to α_m (hexagonal close-packed) transformation led to the formation of a variety of patch-shaped massive grains, including large grain-boundary-crossing grains with misorientations being as much as 30°. Marked transformations have been identified in laser welding of stainless steels where the influence of composition and cooling rate on the solid-state transformation to γ-austenite was studied [126]. An analysis by D'amato et al. [127] showed that grain refinement at the weld area occurred and that δ-ferrite was present in the as-welded samples. The authors also concluded that the welds solidified by primary ferrite solidification with some chromium carbide precipitates in the weld area. The microstructure of the weld metal of a duplex stainless steel made with Nd:YAG pulsed laser was studied by Mirakhorli et al. [128]. They found the weld microstructure to be composed of two distinct zones: (1) at high overlapping factors, an array of continuous axial grains at the weld centerline was formed, and (2) at low overlapping factors, in the zone of higher cooling rate, a higher percentage of ferrite was transformed to austenite. They concluded that the high cooling rates involved in pulsed laser welding led to low overlapping, thus limiting the ferrite-to-austenite transformation to the grain boundaries only.

Concerning other ferrous-based alloys, Babu et al. [129] studied the primary solidification phase of Fe-C-Al-Mn steel welds under rapid and slow cooling rates. They found nonequilibrium austenite solidification during rapid cooling in contrast to equilibrium δ-ferrite solidification that occurs under slow cooling conditions. Nakao et al. [130] studied the effects of rapid solidification by CO_2 laser surface melting of Fe-Cr-Ni ternary alloys. They found rod-like eutectic microstructures that first increased and then decreased with increasing cooling rates. The so-called "massively solidified structures" were formed when the cooling rate exceeded a critical value, which, in turn, is markedly influenced by the chemical composition of the alloy. Microstructurally, the δ-ferrite contents were influenced by the cooling rate.

El-Batahgy [30] evaluated the fusion zone shape and solidification structure as a function of laser welding parameters. He found that the type of the fusion zone microstructure does not depend on the change in heat input, and it is always austenite, with ~2-3 vol.% ferrite. However, a finer solidification structure could be obtained by lowering the heat input.

Mohanty and Mazumder [131] observed the solidification behavior of the melt-pool during laser melting and stated that the keyhole shape influences the flow pattern in the melt-pool, which may change the microstructure characteristics. Even under constant scanning speed conditions, they observed an unsteady motion of the solid-liquid interface, resulting in fluctuation in growth rates and in thermal fields, which makes a solidified zone remelt and resolidify. This leads to discrete structural bands in the solidified bead. Using time-resolved X-ray diffraction, David et al. [132] analyzed the instabilities at the solid-liquid interface and confirmed that, on slowly cooled spot welds, the equilibrium primary solidification phase is δ-ferrite but, in rapid solidification, primary austenite was observed. Using momentum, continuity, and energy equations for incompressible, laminar, and Newtonian flow, Roy et al. [133] developed a model to simulate the temperature and velocity fields during pulsed laser welding and verified it using experimental results [134]. The computed cooling rates and weld bead dimensions were consistent with experimental results. However, the ratio of the temperature gradient to the solidification rate indicated that conditions for plane front solidification of stainless steel were not satisfied for the pulsed laser welding parameters. Therefore, these workers suggested that numerical calculations could improve understanding of solidification during pulsed laser welding.

The role of the shape of the melt-pool on the weld microstructure has been studied by Rappaz et al. [135], who created a three-dimensional reconstruction of the electron beam weld-pool shape and measured dendrite spacing as a function of growth velocity. The dendrites were found to grow parallel to three <100> crystallographic directions, which indicated that dendrites that occurred from the single crystal portion remained solid during the welding process. The weld microstructure contained dendrites that were only slightly branched and had a cell-like structure. David and Vitek [136] were the first one to observe the effect of cooling rate on the modification of microstructure from austenite + ferrite to fully austenitic structure in austenitic stainless steels. They determined that this was due to a large undercooling encountered by the liquid under rapid cooling conditions encountered during electron and laser beam welding. Here, two phenomena occur as solidification growth velocities increase: (1) partitioning of the solute between solid and liquid and (2) nonequilibrium phase formation. Kelly et al. [137] made similar observations in their study of rapid solidification of 303 stainless steel droplets and found that solute elements were more

completely trapped in the bcc structures. The crystal-to-liquid nucleation temperatures showed that bcc nucleation was favored at large liquid supercooling. More recently, Siefert and David [138] studied the weldability of austenitic stainless steels and attributed changes in the microstructure to large undercooling in the liquid and partitionless solidification.

Hu and Richardson [139] evaluated the cracking behavior in welds of high-strength Al alloys and found out that cracking happens when the fusion zone is in the semisolid state and it is related to the temperature distribution, which is elongated in the welding direction. These workers confirmed that this temperature distribution during the cooling phase causes a transverse tensile strain in the fusion zone. To avoid cracking, they suggested three solutions: decrease the scanning speed in order to decrease the longitudinal strain, alter the composition in the fusion zone to improve the strength and ductility of the weld, and add a heating or cooling source to modify the thermal history of the fusion zone in the semisolid temperature range. Rai et al. [140] stated that the values of solidification parameters at the trailing edge of the melt-pool depend on the physical properties of the material, with some very influential ones being thermal diffusivity, absorption coefficient, melting temperature, and boiling temperature. Materials with a lower thermal conductivity are expected to have a fusion zone, which is spread near the top. A number of workers have combined various existing models that consider multiple beam reflections in the keyhole to calculate temperature and velocity fields, weld geometry, and solidification parameters during laser welding of tantalum, Ti-6Al-4V, 304L stainless steel, and vanadium [4, 25, 53, 56, 62, 65, 141–150]. In addition, these researchers used a turbulence model to calculate the thermal conductivity and effective viscosity in the melt-pool. They confirmed that the main mechanism of heat transfer for all four materials was convective heat transfer that depends on the thermal diffusivity and temperature coefficient of surface tension. The smallest melt-pool was observed in tantalum, a consequence of its high boiling temperature, melting temperature, and solid-state thermal diffusivity.

Ghaini et al. [151] conducted experiments to examine the influence of process parameters on the microstructure and hardness during overlap laser bead-on-plate spot welding. They defined the effective peak power density that takes into account the effect of overlapping. They presented two approaches for full-penetration welding: high peak power densities with high travel speeds that have low overlapping and medium peak power densities with medium travel speeds. In the first approach, due to the higher cooling rates and the nature of the thermal effects of the next pulse on the previous weld spot, the weld metal has high hardness and displayed large hardness variation, while opposite results were obtained when the latter approach was used. Combining these two approaches and having the optimum power density with overlapping factor enhances prediction of the weld microstructure and hardness. In a bid to understand the hot cracking phenomena in laser overlap spot welding of Al alloys, Ghaini et al. [151] investigated the interdependency of solidification cracking in the weld metal with liquation cracking in the base metal and concluded that the liquation cracks act as initiation sites for solidification cracks. However, at low laser pulse energies, liquation grain boundary cracks occur less frequently and solidification cracks initiate independently from the fusion lines between subsequent weld spots. These workers stated that cracks could only occur when the rate of induced strains was greater than the rate of backfilling.

Kadoi et al. [152] studied the influence of welding speed on solidification cracking susceptibility in laser welding of type 310S stainless steel and found that an increase in welding speed decreases the critical strain for solidification crack initiation. They suggested the reason to be the distribution morphology of the residual liquid at the weld bead center that depends on the microstructure at the rear of the melt-pool. Tan and Shin [153] presented a multiscale model of solidification and microstructure development during laser keyhole welding of austenite stainless steel. On a macroscale, a model was utilized to predict the fluid flow, thermal history, and solidification conditions of the melt-pool, which is influenced by the welding speed. The mesoscale model was used to predict the grain growth in welds, and the macroscale model was developed to simulate the dendrite growth. These workers observed that grain growth direction varies according to the melt-pool complex shape. The maximum temperature gradient controls the dendrite orientation, while the dendrite morphology is influenced by the cooling rate. Increasing the cooling rate reduces the spacing of the primary dendrite arms and suppresses the growth of the secondary dendrite arms. A summary of microstructural development as a function of cooling rate is presented in Table 3.

6. Weld Porosity

Porosity is especially important in Mg and Al alloys, and researchers have conducted several experiments on these two metal alloys in order to determine the porosity characteristics of the melt-pool in the keyhole laser welding process. In recent years, Mg and its alloys have gained increasing interest in industry, mainly due to their low density [155]. Furthermore, liquid Mg has a much larger solubility of hydrogen than solid Mg [156]. Therefore, hydrogen porosity is an important concern for the welding of Mg alloys [157]. Galun and Mordike [49] observed a large number of pores in welds of high-pressure die-cast alloys, such as AZ 91 and AM 60, due to escaping gas entrapped in the material during the die casting process. Through experiments, Pastor et al. [41] showed that overfill on the AM60B alloy weld was caused by the displacement of liquid metal by the pores. Therefore, any parameter that reduces porosity in the melt-pool decreases overfill. They showed that expansion of the initial pores in the base metal is the most important mechanism of porosity formation. For this alloy, Zhao and DebRoy [47] came to the same conclusion. They observed that coalescence and expansion of the initial pores, due to heating and reduction of internal pressure, play a key role in increasing the porosity in the fusion zone. They asserted that a balance between surface tension pressure and vapor pressure determines the stability

Table 3: Effect of the solidification rate on the microstructure of metals and alloys.

Cooling rate ($K \cdot s^{-1}$)	10^5	10^4	10^3	10^2	10^1
Microstructural features	Amorphous	Fine grains	Fine dendrites	Martensite [154]	Dendrites [132]
Comments	Metastable	Nonequilibrium	None	None	Follows equilibrium-phase diagram

of the keyhole. However, pore formation during laser welding of alloy AM60B does not depend on the keyhole instability.

The 2000, 5000, and 6000 series Al alloys are used in many automotive applications, such as body panels, because of the combination of high specific strength, good crashworthiness, and excellent corrosion resistance [158]. These attributes make laser beam welding an attractive joining process for such applications [159, 160]. However, porosity, hot cracking, and weld metal composition change are major concerns in the welding of Al alloys [161]. The formation of the keyhole leads to a deep penetration weld, and a hole created in a liquid is unstable by its nature, causing the formation of porosity in the weld metal. Since porosity is one of the serious problems in very high-power laser welding, Matsunawa et al. [5] observed that, in pulsed laser spot welding of Al alloys, the keyhole opening collapses within one-tenth of the time that the melt-pool solidifies and a large cavity forms at the bottom of the keyhole. Fluctuation of the keyhole opening was less unstable in continuous-wave laser than that in pulsed laser. However, the shape and the size of the melt-pool change with time. By observing the keyhole using optical and X-ray methods, they found that a deep depression is formed on the rear wall of the keyhole, moving from the top to the bottom periodically. They also observed a large bubble in the melt-pool, resulting in the formation of pores. The bubble is composed of evaporated metal vapor and entrained shielding gas. These workers observed two types of porosity in laser-welded parts: porosity induced by hydrogen and a large cavity caused by the fluctuation of the keyhole by intense evaporation of the metal. They also found two effective methods for reducing porosity in Al alloys: use of a low-dew point shielding gas below 250°C and removal of the oxide layer from the surface. The cavity formation in pulsed laser spot welding can be suppressed by adding a proper tailing pulse to avoid collapse of the keyhole opening. In continuous-wave laser welding of Al alloys, Matsunawa et al. [5] found N_2 shielding to be effective in suppressing large pores. This is because of the formation of aluminum nitride (AlN) on the liquid surface, which suppresses the perturbation of both the melt-pool and the keyhole. Moreover, entrained N_2 in the keyhole is consumed, forming AlN; therefore, the number of shielding gas-filled pores is reduced.

Mizutani et al. [51] irradiated a laser beam to the surface of a solid metal and to an already molten metal and observed that the keyhole initiates much earlier in the molten metal than it does in the solid metal. They presented a simplified numerical calculation demonstrating that the formation of bubbles is influenced by surface tension. They showed that the deepest location of the keyhole tends to collapse more easily. Therefore, formation of the bubbles in deep and narrow keyholes is expected. Courtois et al. [162] confirmed that, in pulsed laser welding with a high laser power, when the laser beam is not being applied, the keyhole wall collapses and entraps some gas, creating bubbles, which, in turn, lead to pores. In addition to resolidification microstructures, defects, such as voids, form. Kim and Weinman [163] irradiated samples of 2024-T3-51 Al with a pulsed Nd-glass 1.06 μm laser at an incident energy density of 440 $J \cdot cm^{-2}$, with and without a protective helium gas flow over the surface. A cooling rate of 105 to 107 $K \cdot s^{-1}$ was estimated. They found that many elongated and small voids formed at the melt-matrix interface due to a combination of shrinkage and gas expulsion and that void presence reduced fracture resistance. These authors determined that gas ejection in the melt affected dendrites' growth patterns.

In a computational fluid dynamics study, Zhao et al. [164] considered the existence of the three phases of the material and employed continuity, energy, and momentum equations. They extrapolated the material properties for high temperatures and assumed the fluid to be Newtonian and the flow to be laminar and incompressible. They reported the main cause of the porosity defect to be the oscillation of the keyhole depth, while the depth of the melt-pool is steady. The keyhole oscillates due to the opposition of the dynamic forces and the melt flow. Courtois et al. [165] confirmed the findings by Zhao et al. by calculating the laser reflections in the keyhole during laser welding. They used Maxwell equations, coupled with continuity, energy, and momentum equations, to develop a model for calculating the laser reflections in the process. Moreover, they showed that the shear stress at the keyhole surface has a marked influence on the melt-pool dynamics. Cho et al. [166] simplified the laser welding process by assuming a void region for the region of gas or plasma. They modified the laser beam model they used in their previous work [167], in which an infinitesimal point was considered as the focal point on the surface. In the later model, the focal point was calculated and the reflections were taken into account. Through the use of mass, energy conservation, and the Navier–Stokes equations, they considered buoyancy and Marangoni forces as well as recoil pressure. They confirmed that using a beam with a Gaussian profile could lead to reliable results, and they observed that consideration of the shear stress on the keyhole wall, which is generated by the metal vapor, does not play a significant role in the shape of the HAZ.

7. Summary

The present work is a state-of-the-art literature review on the properties of the melt-pool in laser welding and the relationship between welding process parameters and melt-pool characteristics. The characteristics considered were

geometry, thermodynamics, fluid dynamics, microstructure, and porosity. Furthermore, the optimum laser welding parameters for a selection of metals and alloys are presented in this review. Several experimental studies have been conducted on melt-pool characterization in laser welding. However, direct experimental observation of melt-pool characteristics remains a challenge because of the high temperatures in the melt-pool and the difficulty of monitoring the metal vapor in the keyhole. Thus, there is scope for developing more sophisticated experimental techniques. A number of models, having varying degrees of sophistication, have been used. Four common shortcomings of many of these models are identified. First, simplifications were used; for instance, the temperature dependence of the thermophysical properties of materials is either neglected or extrapolated for high temperatures. Second, the influence of consideration of the three heat transfer modes, namely, conduction, convection, and radiation, in both the radial and the axial directions in the melt-pool, has received little attention. Third, fluid flow in the melt-pool is considered incompressible and laminar. Fourth, the agreement between model and experimental results is not very good. These observations suggest a number of areas for future study. For example, models may be improved by taking into account the compressibility of the vapor in the keyhole and the turbulence of the fluid flow in the melt-pool. In terms of models, multiscale models, which integrate nanostructures and microstructures of materials with multiphysics macroscale models, are needed. Additionally, more experimental results are needed on a wide collection of alloys and welding parameters, yielding results that would enhance verification and validation of models.

Appendix

Several experimental and modeling studies have been performed to understand the influence of process parameters on melt-pool and keyhole features. This appendix contains summaries of a number of these studies.

Chande and Mazumder [7] evaluated the influence of process parameters on the melt-pool shape and cooling rates. They used a finite difference model for the heat source and assumed a quasi-steady state model and observed that when a surface reflectivity is very high, there is no melting; however, as surface melting occurs, surface reflectivity variation has no influence on other process parameters. Therefore, in their model, at the temperatures higher than the melting temperature, the surface reflectivity is considered zero. They concluded that the depth of the penetration is more affected than the width of the weld by the absorption of laser energy in the keyhole. Lankalapalli et al. [31] presented a two-dimensional heat conduction model (heat conduction in the axial direction is neglected) to estimate the dependence of penetration depth on process parameters. They obtained the depth of penetration by equating the conducted heat in the substrate to the absorbed laser power.

The interdependency between the melt-pool and the keyhole has been investigated. Ducharme et al. [42] presented an integrated model of laser welding, taking into account the conditions in the keyhole as well as in the melt-pool, interactively. These authors investigated the influence of process parameters on the melt-pool shape. Whether penetration was full, partial, or blind, the melt-pool shape was different. However, their model is applicable only for full penetration. They concluded that a change in process parameters has more influence on the length of the melt-pool than on its width or shape.

To simulate the laser penetration welding process, Sudnik et al. [150] considered the keyhole, the melt-pool, and the solid substrate as a single nonlinear thermodynamic continuum and divided the whole process to submodels for laser beam, plasma formation, radiation absorption, vapor channel, melt-pool, and solid substrate. This allowed them to calculate the keyhole and melt-pool geometries and temperature distribution, as well as energy losses due to, for example, reflection, vaporization, and radiation. In a later contribution, Sudnik et al. [32] enhanced this model by suggesting a correlation between the depth and the length of the melt-pool. They added the consideration of heat transport due to the moving flow in the radial direction. In the case of a constant welding speed with a varying laser power, they suggested a linear correlation between the depth and the length of the melt-pool. These authors also investigated laser welding of overlap joints [168] and suggested a low welding speed in cases of larger gap widths so that there would be time for the heat to expand through the gap more uniformly.

Butt welding is a technique used to connect parts that are nearly parallel and do not overlap. Benyounis et al. [12] investigated laser butt welding and developed linear and quadratic-fitted polynomial equations for predicting the heat input and the weld bead geometry. They asserted that achieving the maximum penetration is possible by using the maximum laser power with a focused beam while the welding speed is minimum. They confirmed that the most important factors affecting the welded zone width are the welding speed and the laser focal point position. Shanmugam et al. [33] carried out experiments in which they obtained excellent weld bead geometry by selecting an effective combination of input parameters and radiating the laser beam with different angles to the specimen surface.

To better understand the behavior of steel during the welding process, Mei et al. [34] constructed a setup to avoid most of the defects such as pores and cracks in the HAZ by optimizing the process parameters. They also determined various mechanical properties of the alloy and the welded joints. Based on the results of these tests, they confirmed that both the yield strength and the tensile strength of the welded joints are higher than those of the base metal. They stated that, by moving the focal point position down to the depth, melt-pool depth increases at first and then decreases. To understand the effects of laser power, welding speed, and fiber diameter on bead geometry and mechanical properties of the weld, Khan et al. [35] conducted an experimental investigation of laser beam welding in a constrained overlap configuration. They found that welding speed and laser power are the most significant factors that influence weld bead geometry. By increasing the energy density input, the

bead profile shape changes from conical to cylindrical. In another study, Khan et al. [169] presented an experimental design approach to process parameter optimization. They developed a set of mathematical models to obtain the graphical optimization of the results and thus the optimal parameters.

The low density, excellent high-temperature mechanical properties, and good corrosion resistance of Ti and its alloys have led to successful applications of these materials in a variety of fields, such as the medical, aerospace, automotive, petrochemical, nuclear, and power generation industries [50, 170]. Fusion welding of Ti has been performed principally using inert gas-shielded arc and high-energy beam welding processes. Laser welding of Ti-6Al-4V alloy is widely used in aerospace and other applications. Casalino et al. [50] investigated laser welding of Ti-6Al-4V alloy using either lap or butt configurations and obtained the process parameters that lead to welds with the minimal number of imperfections. A pulsed and continuous-wave mode laser has been used to weld Ti alloys. In pulse-mode laser welding, the most important parameter affecting the penetration depth is the peak power of the pulsed laser [36]. If it is too high, it creates vapors on the surface of the material, preventing the laser beam from reaching the material, and the penetration depth remains constant. Therefore, for increasing the penetration depth while preventing creation of vapor craters, the peak power should be kept constant and the pulse duration should be increased. These researchers illustrated the relationship between peak power, HAZ width, and melt-pool width: the higher the peak power, the higher the transfer of heat energy to the keyhole walls and the higher the proportion between the HAZ width and the melt-pool width [36]. In order to determine the influence of the heat input on the quality of the welded joint, Quan et al. [37] carried out experiments and showed that, by increasing the heat input, the widths at the top and at the bottom of the weld become equal and more craters and pores are created. Combining various models and concepts, such as multiple reflections of the laser beam in the keyhole, Al-Kazzaz et al. [38] calculated the geometry of the keyhole and weld profiles as well as the temperature gradient in the melt-pool.

Shercliff and Ashby [171] developed a model involving both Gaussian and non-Gaussian heat sources. This enhanced model is applicable for all practical beam speeds. They also presented process diagrams, in a combined form called a "Master Diagram," for rectangular heat sources so that process variables could be selected to achieve optimum results. Steen et al. [172] presented a simple relation between the penetration depth and the process parameters using a one-dimensional conduction balance without radiative heat transfer. They assumed that the material properties are constant for all temperature ranges and claimed that the state of the convection in the melt-pool does not affect the prediction of the depth of the pool. Ahmed et al. [39] used three heat sources to investigate the effect of heat source on the melt-pool shape in laser welding of Inconel 625. The heat sources were a single circular Gaussian beam and two superimposed multiple Gaussian heat sources forming a rectangular beam and one made up of three laser beams and the other of ten beams. The melt-pool profiles modeled using rectangular beams agreed with the experimental results, considering the dependence on the scanning speed. These profiles have a top-hat shape at higher speeds and a crescent shape at lower speeds, as is seen experimentally.

Chan et al. [24] used nondimensional forms of the energy, continuity, and momentum equations and found the highest fluid velocity and the solidification start position at the edge of the beam due to the maximum temperature gradient at this point. The width-to-depth ratio of the melt-pool increases with the increase in Pr. The increase of this ratio with the increase of the surface tension number was not uniform; specifically, it increased up to surface tension number of 55,000 and then it decreased. To evaluate the shape of the melt-pool, Sonti and Amateau [173] solved a nonlinear heat conduction model using FEA and calculated the temperature distribution in the melt-pool. The results were comparable to the results of the experiments that Sonti [174] had carried out to evaluate the influence of the process parameters on laser welding of Al alloys.

Conflicts of Interest

The authors declare that there are no conflicts of interest.

Acknowledgments

The authors thank the FedEx Institute of Technology, The University of Memphis, Memphis, TN, USA, for partial funding of this work under the DRONES cluster.

References

[1] Lasers—high-power and low-power," *Optics & Laser Technology*, vol. 3, no. 3, pp. 181–185, 1971.

[2] J. Mazumder, "Laser welding: state of the art review," *JOM*, vol. 34, no. 7, pp. 16–24, 1982.

[3] M. S. Brown and C. B. Arnold, "Fundamentals of laser-material interaction and application to multiscale surface modification," *Laser Precision Microfabrication. Springer Series in Materials Science*, vol. 135, pp. 91–120, Springer, Berlin, Germany, 2010.

[4] J. Mazumder and W. M. Steen, "Heat transfer model for cw laser material processing," *Journal of Applied Physics*, vol. 51, no. 2, pp. 941–947, 1980.

[5] A. Matsunawa, J. D. Kim, N. Seto, and M. Mizutani, "Dynamics of keyhole and molten pool in laser welding," *Journal of Laser Applications*, vol. 10, no. 6, pp. 247–254, 1998.

[6] P. Okon, G. Dearden, K. Watkins, M. Sharp, and P. French, "Laser welding of aluminium alloy 5083," in *Proceedings of the 21st International Congress Applications of Lasers Electro-Optics*, vol. 53, pp. 1689–1699, Scottsdale, AZ, USA, October 2002.

[7] T. Chande and J. Mazumder, "Estimating effects of processing conditions and variable properties upon pool shape, cooling rates, and absorption coefficient in laser welding," *Journal of Applied Physics*, vol. 56, no. 7, pp. 1981–1986, 1984.

[8] T. Zacharia, S. A. David, J. M. Vitek, and T. Debroy, "Heat transfer during Nd-Yag pulsed laser welding and its effect on solidification structure of austenitic stainless steels," *Metallurgical Transactions A*, vol. 20, no. 5, pp. 957–967, 1989.

[9] L. X. Yang, X. F. Peng, and B. X. Wang, "Numerical modeling and experimental investigation on the characteristics of molten pool during laser processing," *International Journal of Heat and Mass Transfer*, vol. 44, no. 23, pp. 4465–4473, 2001.

[10] K. Abderrazak, S. Bannour, H. Mhiri, G. Lepalec, and M. Autric, "Numerical and experimental study of molten pool formation during continuous laser welding of AZ91 magnesium alloy," *Computational Materials Science*, vol. 44, no. 3, pp. 858–866, 2009.

[11] M. Dhahri, J. E. Masse, J. F. Mathieu, G. Barreau, and M. Autric, "Laser welding of AZ91 and WE43 magnesium alloys for automotive and aerospace industries," *Advanced Engineering Materials*, vol. 3, no. 7, pp. 504–507, 2001.

[12] K. Y. Benyounis, A. G. Olabi, and M. S. J. Hashmi, "Effect of laser welding parameters on the heat input and weld-bead profile," *Journal of Materials Processing Technology*, vol. 164-165, pp. 978–985, 2005.

[13] R. Morgan, C. J. Sutcliffe, and W. O'neill, "Density analysis of direct metal laser re-melted 316L stainless steel cubic primitives," *Journal of Materials Science*, vol. 39, no. 4, pp. 1195–1205, 2004.

[14] W. M. Steen, *Laser Material Processing*, Springer Verlag, London, UK, 1st edition, 1991.

[15] E. Locke, E. D. Hoag, and R. Hella, "Deep penetration welding with high-power CO_2 lasers, quantum electron," *IEEE Journal of Quantum Electronics*, vol. 8, no. 2, pp. 132–135, 1972.

[16] J. Mazumder, "An overview of melt dynamics in laser processing," in *International Society for Optics and Photonics*, E.-W. Kreutz, A. Quenzer, and D. Schuoecker, Eds., pp. 228–241, 1987.

[17] S. A. David and J. M. Vitek, "Correlation between solidification parameters and weld microstructures," *International Materials Reviews*, vol. 34, no. 1, pp. 213–245, 1989.

[18] X. Cao, W. Wallace, and C. Poon, "Research and progress in laser welding of wrought aluminum alloys. I. Laser welding processes," *Materials and Manufacturing Processes*, vol. 18, no. 1, pp. 1–22, 2003.

[19] X. Cao, W. Wallace, and J. P. Immarigeon, "Research and progress in laser welding of wrought aluminum alloys. II. Metallurgical microstructures, defects, and mechanical properties," *Materials and Manufacturing Processes*, vol. 18, no. 1, pp. 23–49, 2003.

[20] J. Shao and Y. Yan, "Review of techniques for on-line monitoring and inspection of laser welding," *Journal of Physics: Conference Series*, vol. 15, pp. 101–107, 2005.

[21] X. Cao, M. Jahazi, J. P. Immarigeon, and W. Wallace, "A review of laser welding techniques for magnesium alloys," *Journal of Materials Processing Technology*, vol. 171, no. 2, pp. 188–204, 2006.

[22] L. Liu, D. Ren, and F. Liu, "A review of dissimilar welding techniques for magnesium alloys to aluminum alloys," *Materials*, vol. 7, no. 5, pp. 3735–3757, 2014.

[23] W. M. Steen, "Laser surface treatment," in *Laser Material Processing*, pp. 172–219, Springer, London, UK, 1991.

[24] C. Chan, J. Mazumder, and M. M. Chen, "A two-dimensional transient model for convection in laser melted pool," *Metallurgical Transactions A*, vol. 15, no. 12, pp. 2175–2184, 1984.

[25] V. V. Semak and A. Matsunawa, "The role of recoil pressure in energy balance during laser materials processing," *Journal of Physics D: Applied Physics*, vol. 30, no. 18, pp. 2541–2552, 1997.

[26] A. P. Mackwood and R. C. Crafer, "Thermal modelling of laser welding and related processes: a literature review," *Optics & Laser Technology*, vol. 37, no. 2, pp. 99–115, 2005.

[27] A. Yaghi and A. A. Becker, "Weld Simulation using Finite Element Methods," in *Proceedings of the NAFEMS World Congress*, St Julians, Malta, May 2005.

[28] X. He, "Finite element analysis of laser welding: a state of art review," *Materials and Manufacturing Processes*, vol. 27, no. 12, pp. 1354–1365, 2012.

[29] J. Svenungsson, I. Choquet, and A. F. H. Kaplan, "Laser welding process–a review of keyhole welding modelling," *Physics Procedia*, vol. 78, pp. 182–191, 2015.

[30] A. M. El-Batahgy, "Effect of laser welding parameters on fusion zone shape and solidification structure of austenitic stainless steels," *Materials Letters*, vol. 32, no. 2-3, pp. 155–163, 1997.

[31] K. N. Lankalapalli, J. F. Tu, and M. Gartner, "A model for estimating penetration depth of laser welding processes," *Journal of Physics D: Applied Physics*, vol. 29, no. 7, pp. 1831–1841, 1996.

[32] W. Sudnik, D. Radaj, S. Breitschwerdt, and W. Erofeew, "Numerical simulation of weld pool geometry in laser beam welding," *Journal of Physics D: Applied Physics*, vol. 33, no. 6, p. 662, 2000.

[33] S. Shanmugam, "Numerical and experimental investigation of laser beam welding of AISI 304 stainless steel sheet," *Advances in Production Engineering & Management*, vol. 3, pp. 93–105, 2008.

[34] L. Mei, G. Chen, X. Jin, Y. Zhang, and Q. Wu, "Research on laser welding of high-strength galvanized automobile steel sheets," *Optics and Lasers in Engineering*, vol. 47, no. 11, pp. 1117–1124, 2009.

[35] M. M. A. Khan, L. Romoli, M. Fiaschi, F. Sarri, and G. Dini, "Experimental investigation on laser beam welding of martensitic stainless steels in a constrained overlap joint configuration," *Journal of Materials Processing Technology*, vol. 210, no. 10, pp. 1340–1353, 2010.

[36] E. Akman, A. Demir, T. Canel, and T. Sinmazçelik, "Laser welding of Ti6Al4V titanium alloys," *Journal of Materials Processing Technology*, vol. 209, no. 8, pp. 3705–3713, 2009.

[37] Y. J. Quan, Z. H. Chen, X. S. Gong, and Z. H. Yu, "Effects of heat input on microstructure and tensile properties of laser welded magnesium alloy AZ31," *Materials Characterization*, vol. 59, no. 10, pp. 1491–1497, 2008.

[38] H. Al Kazzaz, M. Medraj, X. Cao, and M. Jahazi, "Nd:YAG laser welding of aerospace grade ZE41A magnesium alloy: modeling and experimental investigations," *Materials Chemistry and Physics*, vol. 109, no. 1, pp. 61–76, 2008.

[39] N. Ahmed, K. T. Voisey, and D. G. McCartney, "Investigation into the effect of beam shape on melt pool characteristics using analytical modelling," *Optics and Lasers in Engineering*, vol. 48, no. 5, pp. 548–554, 2010.

[40] R. Fabbro, S. Slimani, I. Doudet, F. Coste, and F. Briand, "Experimental study of the dynamical coupling between the induced vapour plume and the melt pool for Nd–Yag CW laser welding," *Journal of Physics D: Applied Physics*, vol. 39, no. 2, pp. 394–400, 2006.

[41] M. Pastor, H. Zhao, and T. DebRoy, "Continuous wave-Nd: yttrium–aluminium–garnet laser welding of AM60B magnesium alloys," *Journal of Laser Applications*, vol. 12, no. 3, pp. 91–100, 2000.

[42] R. Ducharme, K. Williamss, P. Kapadia, J. Dowden, B. Steent, and M. Glowackit, "The laser welding of thin metal sheets: an integrated keyhole and weld pool model with supporting experiments," *Journal of Physics D: Applied Physics*, vol. 27, no. 8, pp. 1619–1627, 1994.

[43] C. Limmaneevichitr and S. Kou, "Experiments to simulate effect of Marangoni convection on weld pool shape," *Welding Journal*, vol. 79, pp. 231s–237s, 2000.

[44] P. A. A. Khan and T. Debroy, "Alloying element vaporization and weld pool temperature during laser welding of AlSl 202 stainless steel," *Metallurgical Transactions B*, vol. 15, no. 4, pp. 641–644, 1984.

[45] H. Ki, J. Mazumder, and P. S. Mohanty, "Modeling of laser keyhole welding: part II. simulation of keyhole evolution, velocity, temperature profile, and experimental verification," *Metallurgical and Materials Transactions A*, vol. 33, no. 6, pp. 1831–1842, 2002.

[46] H. Zhao and T. Debroy, "Weld metal composition change during conduction mode laser welding of aluminum alloy 5182," *Metallurgical and Materials Transactions B*, vol. 32, no. 1, pp. 163–172, 2001.

[47] H. Zhao and T. DebRoy, "Pore formation during laser beam welding of die-cast magnesium alloy AM60B-mechanism and remedy," *Welding Journal*, vol. 80, pp. 204–210, 2001.

[48] S. Postma, R. G. K. M. Aarts, J. Meijer, and J. B. Jonker, "Penetration control in laser welding of sheet metal," *Journal of Laser Applications*, vol. 14, no. 4, p. 210, 2002.

[49] A. Weisheit, R. Galun, and B. L. Mordike, "CO_2 laser beam welding of magnesium-based alloys," *Welding Journal*, vol. 77, pp. 149–154, 1998.

[50] G. Casalino, F. Curcio, and F. M. C. Minutolo, "Investigation on Ti6Al4V laser welding using statistical and Taguchi approaches," *Journal of Materials Processing Technology*, vol. 167, no. 2-3, pp. 422–428, 2005.

[51] M. Mizutani, S. Katayama, and A. Matsunawa, "Observation of molten metal behavior during laser irradiation—basic experiment to understand laser welding phenomena," in *Proceedings of the First International Symposium on High-Power Laser Macroprocessing*, pp. 208–213, Osaka, Japan, May 2002.

[52] M. F. Ashby and K. E. Easterling, "The transformation hardening of steel surfaces by laser beams-I. Hypo-eutectoid steels," *Acta Metallurgica*, vol. 32, no. 11, pp. 1935–1948, 1984.

[53] J. Dowden, N. Postacioglu, M. Davis, and P. Kapadia, "A keyhole model in penetration welding with a laser," *Journal of Physics D: Applied Physics*, vol. 20, no. 1, pp. 36–44, 1987.

[54] W. M. Steen, J. Dowden, M. Davis, and P. Kapadia, "A point and line source model of laser keyhole welding," *Journal of Physics D: Applied Physics*, vol. 21, no. 8, pp. 1255–1260, 1988.

[55] M. Beck, P. Berger, F. Dausinger, and H. Hugel, "Aspects of keyhole/melt interaction in high speed laser welding," in *Proceedings of the 8th International Symposium of Gas Flow Chemical Lasers*, pp. 769–774, Madrid, Spain, February 1991.

[56] A. Kaplan, "A model of deep penetration laser welding based on calculation of the keyhole profile," *Journal of Physics D: Applied Physics*, vol. 27, no. 9, pp. 1805–1814, 1994.

[57] C. Lampa, A. F. H. Kaplan, and J. Powell, "An analytical thermodynamic model of laser welding," *Journal of Physics D: Applied Physics*, vol. 30, no. 9, pp. 1293–1299, 1997.

[58] E. H. Amara and A. Bendib, "Modelling of vapour flow in deep penetration laser welding," *Journal of Physics D: Applied Physics*, vol. 35, no. 3, pp. 272–280, 2002.

[59] R. Fabbro, F. Coste, S. Slimani, and F. Briand, "Study of keyhole geometry for full penetration Nd-Yag CW laser welding," *Journal of Physics D: Applied Physics*, vol. 38, no. 12, pp. 1881–1887, 2005.

[60] F. Tenner, C. Brock, F. Klampfl, and M. Schmidt, "Analysis of the correlation between plasma plume and keyhole behavior in laser metal welding for the modeling of the keyhole geometry," *Optics and Lasers in Engineering*, vol. 64, pp. 32–41, 2015.

[61] R. Fabbro, "Melt pool and keyhole behaviour analysis for deep penetration laser welding," *Journal of Physics D: Applied Physics*, vol. 43, no. 44, p. 445501, 2010.

[62] N. Postacioglu, P. Kapadia, and M. Davis, "Upwelling in the liquid region surrounding the keyhole in penetration welding with a laser," *Journal of Physics D: Applied Physics*, vol. 20, no. 3, pp. 340–345, 1987.

[63] A. Kar and J. Mazumder, "Mathematical modeling of keyhole laser welding," *Journal of Applied Physics*, vol. 78, no. 11, pp. 6353–6360, 1995.

[64] X. Ye and X. Chen, "Three-dimensional modelling of heat transfer and fluid flow in laser full-penetration welding," *Journal of Physics D: Applied Physics*, vol. 35, no. 10, pp. 1049–1056, 2002.

[65] J. Goldak, A. Chakravarti, and M. Bibby, "New finite element model for welding heat sources," *Metallurgical Transactions B*, vol. 15, no. 2, pp. 299–305, 1984.

[66] R. Wang, Y. Lei, and Y. Shi, "Numerical simulation of transient temperature field during laser keyhole welding of 304 stainless steel sheet," *Optics & Laser Technology*, vol. 43, no. 4, pp. 870–873, 2011.

[67] C. W. Hirt and B. D. Nichols, "Volume of fluid (VOF) method for the dynamics of free boundaries," *Journal of Computational Physics*, vol. 39, no. 1, pp. 201–225, 1981.

[68] M. Akbari, S. Saedodin, D. Toghraie, R. Shoja Razavi, and F. Kowsari, "Experimental and numerical investigation of temperature distribution and melt pool geometry during pulsed laser welding of Ti6Al4V alloy," *Optics & Laser Technology*, vol. 59, pp. 52–59, 2014.

[69] M. R. Frewin and D. A. Scott, "Finite element model of pulsed laser welding," *Welding Journal*, vol. 78, pp. 15s–22s, 1999.

[70] A. De, S. K. Maiti, C. A. Walsh, and H. K. D. H. Bhadeshia, "Finite element simulation of laser spot welding," *Science and Technology of Welding and Joining*, vol. 8, no. 5, pp. 377–384, 2003.

[71] M. M. Collur, A. Paul, and T. Debroy, "Mechanism of alloying element vaporization during laser welding," *Metallurgical Transactions B*, vol. 18, no. 4, pp. 733–740, 1987.

[72] N. Chakraborty and S. Chakraborty, "Modelling of turbulent molten pool convection in laser welding of a copper-nickel dissimilar couple," *International Journal of Heat and Mass Transfer*, vol. 50, no. 9-10, pp. 1805–1822, 2007.

[73] M. C. Tsai and S. Kou, "Marangoni convection in weld pools with a free surface," *International Journal for Numerical Methods in Fluids*, vol. 9, no. 12, pp. 1503–1516, 1989.

[74] S. Safdar, A. J. Pinkerton, L. Li, M. A. Sheikh, and P. J. Withers, "An anisotropic enhanced thermal conductivity approach for modelling laser melt pools for Ni-base super alloys," *Applied Mathematical Modelling*, vol. 37, no. 3, pp. 1187–1195, 2013.

[75] C. R. Heiple, "Mechanism for minor element effect on GTA fusion zone geometry," *Welding Journal*, vol. 61, pp. 975–1025, 1982.

[76] G. Tsotridis, H. Rother, and E. D. Hondros, "Marangoni flow and the shapes of laser-melted pools," *The Science of Nature*, vol. 76, no. 5, pp. 216–218, 1989.

[77] Y. Cheng, X. Jin, S. Li, and L. Zeng, "Fresnel absorption and inverse bremsstrahlung absorption in an actual 3D keyhole during deep penetration CO_2 laser welding of aluminum 6016," *Optics & Laser Technology*, vol. 44, no. 5, pp. 1426–1436, 2012.

[78] L. Schlessinger and J. Wright, "Inverse-bremsstrahlung absorption rate in an intense laser field," *Physical Review A*, vol. 20, no. 5, pp. 1934–1945, 1979.

[79] G. J. Pert, "Inverse bremsstrahlung absorption in large radiation fields during binary collisions-classical theory. II(b). Summed rate coefficients for Coulomb collisions," *Journal of Physics A: Mathematical and General*, vol. 9, no. 10, pp. 1797–1800, 1976.

[80] Y. Zhang, G. Chen, H. Wei, and J. Zhang, "A novel "sandwich" method for observation of the keyhole in deep penetration laser welding," *Optics and Lasers in Engineering*, vol. 46, no. 2, pp. 133–139, 2008.

[81] W. Tan, N. S. Bailey, and Y. C. Shin, "Investigation of keyhole plume and molten pool based on a three-dimensional dynamic model with sharp interface formulation," *Journal of Physics D: Applied Physics*, vol. 46, no. 5, p. 55501, 2013.

[82] T. Zacharia, S. A. David, J. M. Vitek, and T. Debroy, "Weld pool development during GTA and laser beam welding of type 304 stainless steel, part II—experimental correlation," *Welding Journal*, vol. 68, pp. 510–519, 1989.

[83] C. R. Heiple and J. R. Roper, "Effect of selenium on GTAW fusion zone geometry. Small additions of selenium to a stainless steel dramatically increase the depth/width ratio of GTA welds," *Welding Journal*, vol. 60, p. 143, 1981.

[84] S. A. David and T. Debroy, "Current issues and problems in welding science," *Science*, vol. 257, no. 5069, pp. 497–502, 1992.

[85] V. V. Semak, J. A. Hopkins, M. H. Mccay, and T. D. McCay, "Melt pool dynamics during laser welding," *Journal of Physics D: Applied Physics*, vol. 28, no. 12, pp. 2443–2450, 1995.

[86] V. V. Semak, G. A. Knorovsky, and D. O. MacCallum, "On the possibility of microwelding with laser beams," *Journal of Physics D: Applied Physics*, vol. 36, no. 17, p. 2170, 2003.

[87] V. V. Semak, G. A. Knorovsky, D. O. MacCallum, and R. A. Roach, "Effect of surface tension on melt pool dynamics during laser pulse interaction," *Journal of Physics D: Applied Physics*, vol. 39, no. 3, pp. 590–595, 2006.

[88] J.-H. Cho, D. F. Farson, J. O. Milewski, and K. J. Hollis, "Weld pool flows during initial stages of keyhole formation in laser welding," *Journal of Physics D: Applied Physics*, vol. 42, no. 17, p. 175502, 2009.

[89] M. Zhang, G. Chen, Y. Zhou, and S. Li, "Direct observation of keyhole characteristics in deep penetration laser welding with a 10 kW fiber laser," *Optics Express*, vol. 21, no. 17, pp. 19997–20004, 2013.

[90] M. Geiger, K. H. Leitz, H. Koch, and A. Otto, "A 3D transient model of keyhole and melt pool dynamics in laser beam welding applied to the joining of zinc coated sheets," *Production Engineering*, vol. 3, no. 2, pp. 127–136, 2009.

[91] R. Fabbro and K. Chouf, "Dynamical description of the keyhole in deep penetration laser welding," *Journal of Laser Applications*, vol. 12, no. 4, pp. 142–148, 2000.

[92] S. Basu and T. DebRoy, "Liquid metal expulsion during laser irradiation," *Journal of Applied Physics*, vol. 72, no. 8, pp. 3317–3322, 1992.

[93] T. Debroy and S. A. David, "Physical processes in fusion welding," *Reviews of Modern Physics*, vol. 67, no. 1, pp. 85–112, 1995.

[94] E. H. Amara and R. Fabbro, "Modelling of gas jet effect on the melt pool movements during deep penetration laser welding," *Journal of Physics D: Applied Physics*, vol. 41, no. 5, p. 55503, 2008.

[95] R. Fabbro, M. Hamadou, and F. Coste, "Metallic vapor ejection effect on melt pool dynamics in deep penetration laser welding," *Journal of Laser Applications*, vol. 16, no. 1, pp. 16–19, 2004.

[96] R. Fabbro, F. Coste, S. Slimani, and F. Briand, "Analysis of the various melt pool hydrodynamic regimes observed during Cw Nd-YAG deep penetration laser welding," in *Proceedings of the Conference on Lasers and Electro-Optics (CLEO)*, Europe, June 2007.

[97] E. H. Amara, R. Fabbro, L. Achab, F. Hamadi, and N. Mebani, "Modeling of friction on keyhole walls," in *Proceedings of the 23rd International Congress on Applications of Lasers in Electro-Optics*, San Francisco, CA, USA, 2004.

[98] E. H. Amara, R. Fabbro, and F. Hamadi, "Modeling of the melted bath movement induced by the vapor flow in deep penetration laser welding," *Journal of Laser Applications*, vol. 18, no. 1, p. 2, 2006.

[99] L. Li, D. J. Brookfield, and W. M. Steen, "Plasma charge sensor for in-process, non-contact monitoring of the laser welding process," *Measurement Science and Technology*, vol. 7, no. 4, pp. 615–626, 1996.

[100] P. Norman, H. Engström, and A. F. H. Kaplan, "Theoretical analysis of photodiode monitoring of laser welding defects by imaging combined with modelling," *Journal of Physics D: Applied Physics*, vol. 41, no. 19, 2008.

[101] T. C. Nguyen, D. C. Weckman, D. A. Johnson, and H. W. Kerr, "High speed fusion weld bead defects," *Science and Technology of Welding and Joining*, vol. 11, no. 6, pp. 618–633, 2006.

[102] W. Shimada and S. Hoshinouchi, "A study on bead formation by low pressure TIG arc and prevention of under-cut bead," *Journal of Japan Welding Society*, vol. 51, pp. 280–286, 1982.

[103] U. Gratzke, P. D. Kapadia, J. Dowden, J. Kroos, and G. Simon, "Theoretical approach to the humping phenomenon in welding processes," *Journal of Physics D: Applied Physics*, vol. 25, no. 11, pp. 1640–1647, 1992.

[104] J. Xie, "Dual beam laser welding," *Welding Journal*, vol. 81, pp. 223s–230s, 2002.

[105] M. Kern, P. Berger, and H. Hugel, "Magneto-fluid dynamic effects," *Welding Journal*, vol. 79, p. 72s, 2000.

[106] A. Matsunawa and V. V. Semak, "The simulation of front keyhole wall dynamics during laser welding," *Journal of Physics D: Applied Physics*, vol. 30, no. 5, pp. 798–809, 1997.

[107] Y. Kawahito, M. Mizutani, S. Katayama, and S. Steel, "Investigation of high-power fiber laser welding phenomena of stainless steel," *Transactions of JWRI*, vol. 36, pp. 11–16, 2007.

[108] Y. Kawahito, M. Mizutani, and S. Katayama, "High quality welding of stainless steel with 10 kW high power fibre laser," *Science and Technology of Welding and Joining*, vol. 14, no. 4, pp. 288–294, 2009.

[109] T. Ilar, I. Eriksson, J. Powell, and A. Kaplan, "Root humping in laser welding-an investigation based on high speed imaging," *Physics Procedia*, vol. 39, pp. 27–32, 2012.

[110] E. H. Amara and R. Fabbro, "Modeling of humps formation during deep-penetration laser welding," *Applied Physics A*, vol. 101, no. 1, pp. 111–116, 2010.

[111] S. Pang, L. Chen, J. Zhou, Y. Yin, and T. Chen, "A three-dimensional sharp interface model for self-consistent keyhole and weld pool dynamics in deep penetration laser welding," *Journal of Physics D: Applied Physics*, vol. 44, no. 2, p. 25301, 2010.

[112] H. Ki, J. Mazumder, and P. S. Mohanty, "Modeling of laser keyhole welding: Part I. Mathematical modeling, numerical methodology, role of recoil pressure, multiple reflections, and free surface evolution," *Metallurgical and Materials Transactions A*, vol. 33, no. 6, pp. 1817–1830, 2002.

[113] J. Charles and B. Bonnefois, "Super duplex stainless steels: properties and weldability," in *Proceedings of the Conference in Applications of Stainless Steels*, pp. 1108–1121, Stockholm, Sweden, 1992.

[114] D. J. Kotecki, "Ferrite control in duplex stainless steel weld metal," *Welding Journal*, vol. 65, pp. 273s–278s, 1986.

[115] S. Kou, *Welding Metallurgy*, John Wiley & Sons Inc., Hoboken, NJ, USA, 2003.

[116] A. Munitz, "Microstructure of rapidly solidified laser molten AI-4.5 Wt Pct Cu surfaces," *Metallurgical Transactions B*, vol. 16, no. 1, pp. 149–161, 1985.

[117] S. Narasimhan, S. Copley, E. Van Stryland, and M. Bass, "Epitaxial resolidification in laser melted superalloys," *IEEE Journal of Quantum Electronics*, vol. 13, no. 9, p. 814, 1977.

[118] A. Zambon and F. Bonollo, "Rapid solidification in laser welding of stainless steels," *Materials Science and Engineering: A*, vol. 178, pp. 203–207, 1994.

[119] J. C. Lippold and W. F. Savage, "Solidification of austenitic stainless steel weldments: part 2—the effect of alloy composition on ferrite morphology a transition in ferrite morphology occurs as a function of composition and weld cooling rate," *Welding Journal*, vol. 59, pp. 48s–58s, 1980.

[120] T. Zacharia, S. A. David, J. M. Vitek, and T. Debroy, "Weld pool development during GTA and laser beam welding of type 304 stainless steel, part I-theoretical analysis," *Welding Journal*, vol. 68, pp. 499–509, 1989.

[121] J. C. Lippold, "Solidification behavior and cracking susceptibility of pulsed-laser welds in austenitic stainless steels, a shift in solidification behavior under rapid solidification conditions promotes an increase in cracking susceptibility," *Welding Journal*, vol. 73, pp. 129–139, 1994.

[122] V. Kujanpaa, N. Suutala, T. Takalo, and T. Moisio, "Correlation between solidification cracking and microstructure in austenitic and austenitic-ferritic stainless steel welds," *Welding Journal*, vol. 9, pp. 55–75, 1979.

[123] D. J. Kotecki and T. A. Siewert, "WRC-1992 constitution diagram for stainless steel weld metals: a modification of the WRC-1988 diagram," *Welding Journal*, vol. 71, pp. 171–178, 1992.

[124] J. A. Brooks, M. I. Baskes, and F. A. Greulich, "Solidification modeling and solid-state transformations in high-energy density stainless steel welds," *Metallurgical Transactions A*, vol. 22, no. 4, pp. 915–926, 1991.

[125] S. L. Lu, M. Qian, H. P. Tang, M. Yan, J. Wang, and D. H. StJohn, "Massive transformation in Ti–6Al–4V additively manufactured by selective electron beam melting," *Acta Materialia*, vol. 104, pp. 303–311, 2016.

[126] M. J. Perricone, J. N. Dupont, T. D. Anderson, C. V. Robino, and J.R. Michael, "An investigation of the massive transformation from ferrite to austenite in laser-welded Mo-bearing stainless steels," *Metallurgical and Materials Transactions A*, vol. 42, no. 3, pp. 700–716, 2011.

[127] C. D'amato, M. Fenech, S. Abela, J. C. Betts, and J. Buhagiar, "Autogenous laser keyhole welding of AISI 316LTi," *Materials and Manufacturing Processes*, vol. 25, no. 11, pp. 1269–1277, 2010.

[128] F. Mirakhorli, F. M. Ghaini, and M. J. Torkamany, "Development of weld metal microstructures in pulsed laser welding of duplex stainless steel," *Journal of Materials Engineering and Performance*, vol. 21, no. 10, pp. 2173–2176, 2012.

[129] S. S. Babu, J. W. Elmer, J. M. Vitek, and S. A. David, "Time-resolved X-ray diffraction investigation of primary weld solidification in Fe-C-Al-Mn steel welds," *Acta Materialia*, vol. 50, no. 19, pp. 4763–4781, 2002.

[130] Y. Nakao, K. Nishimoto, and W. P. Zhang, "Effects of rapid solidification by laser surface melting on solidification modes and microstructures of stainless steels ," *Transactions in Japan Welding Society*, vol. 19, pp. 100–106, 1988.

[131] P. S. Mohanty and J. Mazumder, "Solidification behavior and microstructural evolution during laser beam—material interaction," *Metallurgical and Materials Transactions B*, vol. 29, no. 6, pp. 1269–1279, 1998.

[132] S. A. David, S. S. Babu, and J. M. Vitek, "Welding: solidification and microstructure," *JOM*, vol. 55, no. 6, pp. 14–20, 2003.

[133] G. G. Roy, J. W. Elmer, and T. DebRoy, "Mathematical modeling of heat transfer, fluid flow, and solidification during linear welding with a pulsed laser beam," *Journal of Applied Physics*, vol. 100, no. 3, p. 34903, 2006.

[134] Y. F. Tzeng, "Effects of operating parameters on surface quality for the pulsed laser welding of zinc-coated steel," *Journal of Materials Processing Technology*, vol. 100, no. 1–3, pp. 163–170, 2000.

[135] M. Rappaz, S. A. David, J. M. Vitek, and L. A. Boatner, "Development of microstructures in Fe−15Ni−15Cr single crystal electron beam welds," *Metallurgical Transactions A*, vol. 20, no. 6, pp. 1125–1138, 1989.

[136] S. A. David and J. M. Vitek, "Laser in metallurgy," in *Proceedings of Metallurgical Society of AIME*, Chicago, IL, USA, February 1981.

[137] T. F. Kelly, M. Cohen, and J. B. Sande, "Rapid solidification of a droplet-processed stainless steel," *Metallurgical Transactions A*, vol. 15, no. 5, pp. 819–833, 1984.

[138] J. A. Siefert and S. A. David, "Weldability and weld performance of candidate austenitic alloys for advanced ultra-supercritical fossil power plants," *Science and Technology of Welding and Joining*, vol. 19, no. 4, pp. 271–294, 2014.

[139] B. Hu and I. M. Richardson, "Mechanism and possible solution for transverse solidification cracking in laser welding of high strength aluminium alloys," *Materials Science and Engineering: A*, vol. 429, no. 1-2, pp. 287–294, 2006.

[140] R. Rai, J. W. Elmer, T. A. Palmer, and T. DebRoy, "Heat transfer and fluid flow during keyhole mode laser welding of tantalum, Ti–6Al–4V, 304L stainless steel and vanadium," *Journal of Physics D: Applied Physics*, vol. 40, no. 18, pp. 5753–5766, 2007.

[141] D. T. Swift Hook and A. E. F. Gick, "Penetration welding with lasers," *Welding Journal*, vol. 52, no. 11, pp. 492s–499s, 1973.

[142] J. G. Andrews and D. R. Atthey, "Hydrodynamic limit to penetration of a material by a high-power beam," *Journal of Physics D: Applied Physics*, vol. 9, no. 15, pp. 2181–2194, 1976.

[143] P. G. Klemens, "Heat balance and flow conditions for electron beam and laser welding," *Journal of Applied Physics*, vol. 47, no. 5, pp. 2165–2174, 1976.

[144] J. Dowden, M. Davis, and P. Kapadia, "Some aspects of the fluid dynamics of laser welding," *Journal of Fluid Mechanics*, vol. 126, no. 1, p. 123, 1983.

[145] P. S. Wei and C. Y. Ho, "Axisymmetric nugget growth during resistance spot welding," *Journal of Heat Transfer*, vol. 112, no. 2, p. 309, 1990.

[146] J. Kroos, U. Gratzke, and G. Simon, "Towards a self-consistent model of the keyhole in penetration laser beam

welding," *Journal of Physics D: Applied Physics*, vol. 26, no. 3, pp. 474–480, 1993.

[147] H. Zhao and T. DebRoy, "Macroporosity free aluminum alloy weldments through numerical simulation of keyhole mode laser welding," *Journal of Applied Physics*, vol. 93, no. 12, pp. 10089–10096, 2003.

[148] R. Rai and T. DebRoy, "Tailoring weld geometry during keyhole mode laser welding using a genetic algorithm and a heat transfer model," *Journal of Physics D: Applied Physics*, vol. 39, no. 6, pp. 1257–1266, 2006.

[149] R. Rai, G. G. Roy, and T. DebRoy, "A computationally efficient model of convective heat transfer and solidification characteristics during keyhole mode laser welding," *Journal of Applied Physics*, vol. 101, no. 5, p. 54909, 2007.

[150] W. Sudnik, D. Radaj, and W. Erofeew, "Computerized simulation of laser beam welding, modelling and verification," *Journal of Physics D: Applied Physics*, vol. 29, no. 11, pp. 2811–2817, 1996.

[151] F. M. Ghaini, M. J. Hamedi, M. J. Torkamany, and J. Sabbaghzadeh, "Weld metal microstructural characteristics in pulsed Nd: YAG laser welding," *Scripta Materialia*, vol. 56, no. 11, pp. 955–958, 2007.

[152] K. Kadoi, A. Fujinaga, M. Yamamoto, and K. Shinozaki, "The effect of welding conditions on solidification cracking susceptibility of type 310S stainless steel during laser welding using an in-situ observation technique," *Welding in the World*, vol. 57, pp. 383–390, 2013.

[153] W. Tan and Y. C. Shin, "Multi-scale modeling of solidification and microstructure development in laser keyhole welding process for austenitic stainless steel," *Computational Materials Science*, vol. 98, pp. 446–458, 2015.

[154] S. K. Dhua, D. Mukerjee, and D. S. Sarma, "Effect of cooling rate on the as-quenched microstructure and mechanical properties of HSLA-100 steel plates," *Metallurgical and Materials Transactions A*, vol. 34, no. 11, pp. 2493–2504, 2003.

[155] D. Thomas, "Increased magnesium usage: not just due to density," *Automobile Engineering*, vol. 99, p. 47, 1991.

[156] H. Baker, *Magnesium and Magnesium Alloys*, ASM international, Materials Park, OH, USA, 1999.

[157] J. D. Shearouse and B. A. Mikucki, *The Origin of Microporosity in Magnesium Alloy A291*, SAE International, Warrendale, PA, USA, 1994.

[158] L. Griffing, "Metals and their weldability," in *Welding Handbook*, American Welding Society, Miami, FL, USA, 1972.

[159] B. Irving, "Blank welding forces automakers to sit up and take notice," *Welding Journal*, vol. 71, pp. 39–45, 1991.

[160] P. A. Hilton, *Optical and Quantum Electronics*, vol. 27, Springer, Berlin, Germany, 1995.

[161] H. Zhao, D. White, and T. DebRoy, "Current issues and problems in laser welding of automotive aluminium alloys," *International Materials Reviews*, vol. 44, no. 6, pp. 238–266, 1999.

[162] M. Courtois, M. Carin, P. Le Masson, S. Gaied, and M. Balabane, "A complete model of keyhole and melt pool dynamics to analyze instabilities and collapse during laser welding," *Journal of Laser Applications*, vol. 26, no. 4, p. 42001, 2014.

[163] C. Kim and L. S. Weinman, "Porosity formation in laser surface melted aluminum alloys," *Scripta Metallurgica*, vol. 12, no. 1, pp. 57–60, 1978.

[164] H. Zhao, W. Niu, B. Zhang, Y. Lei, M. Kodama, and T. Ishide, "Modelling of keyhole dynamics and porosity formation considering the adaptive keyhole shape and three-phase coupling during deep-penetration laser welding," *Journal of Physics D: Applied Physics*, vol. 44, no. 48, p. 485302, 2011.

[165] M. Courtois, M. Carin, P. Le Masson, S. Gaied, and M. Balabane, "A new approach to compute multi-reflections of laser beam in a keyhole for heat transfer and fluid flow modelling in laser welding," *Journal of Physics D: Applied Physics*, vol. 46, no. 50, p. 505305, 2013.

[166] W. I. Cho, S. J. Na, C. Thomy, and F. Vollertsen, "Numerical simulation of molten pool dynamics in high power disk laser welding," *Journal of Materials Processing Technology*, vol. 212, no. 1, pp. 262–275, 2012.

[167] W. I. Cho, S. J. Na, M. H. Cho, and J. S. Lee, "Numerical study of alloying element distribution in CO_2 laser-GMA hybrid welding," *Computational Materials Science*, vol. 49, no. 4, pp. 792–800, 2010.

[168] W. Sudnik, D. Radaj, and W. Erofeew, "Computerized simulation of laser beam weld formation comprising joint gaps," *Journal of Physics D: Applied Physics*, vol. 31, no. 24, pp. 3475–3480, 1998.

[169] M. M. A. Khan, L. Romoli, M. Fiaschi, G. Dini, and F. Sarri, "Experimental design approach to the process parameter optimization for laser welding of martensitic stainless steels in a constrained overlap configuration," *Optics & Laser Technology*, vol. 43, no. 1, pp. 158–172, 2011.

[170] S. H. Wang, M. D. Wei, and L. W. Tsay, "Tensile properties of LBW welds in Ti–6Al–4V alloy at evaluated temperatures below 450°C," *Materials Letters*, vol. 57, no. 12, pp. 1815–1823, 2003.

[171] H. R. Shercliff and M. F. Ashby, "The prediction of case depth in laser transformation hardening," *Metallurgical Transactions A*, vol. 22, no. 10, pp. 2459–2466, 1991.

[172] P. H. Steen, P. Ehrhard, and A. S. Ssler, "Depth of melt-pool and heat-affected zone in laser surface treatments," *Metallurgical and Materials Transactions A*, vol. 25, no. 2, pp. 427–435, 1994.

[173] N. Sonti and M. F. Amateau, "Finite-element modeling of heat flow in deep-penetration laser welds in aluminum alloys," *Numerical Heat Transfer, Part A: Applications*, vol. 16, no. 3, pp. 351–370, 1989.

[174] N. Sonti, *Influence of Process Parameters on Laser Weld Characteristics in Aluminum Alloys*, Pennsylvania State University, State College, PA, USA, 1988.